Open Access



# The Early Bronze Age IA site at Dor South, Carmel Coast, Israel: the economic system of a pre-urban coastal settlement in the eastern Mediterranean

Ruth Shahack-Gross[*, a, b], Roey Nickelsberg[a], Assaf Yasur-Landau[a, b], Isaac Ogloblin Ramirez[a, b], Alyssa V. Pietraszek[a], Shira Gur-Arieh[a, b, c], Ilaria Patania[a, d], Nadya Teutsch[e], Nimrod Marom[a, b], Cheryl A. Makarewicz[f], Gal Bermatov-Paz[a]

[a] Department of Maritime Civilizations, School of Archaeology and Maritime Cultures, University of Haifa, Haifa, Israel
[b] Leon Recanati Institute for Maritime Studies, University of Haifa, Haifa, Israel
[c] Institute for Pre- and Protohistoric Archaeology and Archaeology of the Roman Provinces, Ludwig Maximilian University of Munich, Munich, Germany
[d] Zinman Institute of Archaeology, University of Haifa, Haifa, Israel
[e] The Geological Survey of Israel, Jerusalem, Israel
[f] Archaeological Stable Isotope Laboratory, Institute of Prehistoric and Protohistoric Archaeology, Christian-Albrechts University of Kiel, Kiel, Germany
[*] Corresponding author's email address: rgross@univ.haifa.ac.il

## Keywords

Early Bronze Age I, coastal resources, geoarchaeology, pottery, micromorphology, phytoliths, basalt groundstones, faunal stable isotopes, flint, elemental analysis

## Abstract

Dor South is a shoreline site on the Carmel Coast, currently lying ca. 50 m from the waterfront. Following a survey, an undisturbed area at the northernmost edge of the site (Area A) was excavated during 2018–2020 for a total of six weeks. A 1.0–1.5 m thick stratified accumulation of anthropogenic deposits was revealed in the lee side of a coastal aeolianite ridge resting on an ancient coastal dune. Artifacts include extensive pottery and flint assemblages, some basalt groundstone items, meager faunal remains, and practically no macrobotanical and architectural remains. The purpose of this study is to explore the settlement's socioeconomic nature; the results show that by using a micro-geoarchaeological approach, even a non-architectural settlement's edge yields information that would have remained unknown otherwise. This is especially important given that Dor South is the only large shoreline Early Bronze Age (EB) IA (ca. 3800/3700–3300 BCE) site in the northern part of the Israeli coast, based on pottery typology. The lowermost part of the site includes activity remains also from the Late Neolithic/Early Chalcolithic (Wadi Rabah) period (ca. 5800/5500–4500 BCE). A micro-geoarchaeological analysis of the site's deposits showed a high abundance of grass phytoliths and absence of dung spherulites. A phytolith morphotype analysis indicated a mix of wild grasses and domesticated cereals. Evidence of wood ash occurred only in the lowermost occupation deposits. Geochemistry of the basalt items suggests procurement from outcrops in the nearby Mount Carmel, Jezreel Valley, and possibly the Golan Heights. Faunal remains are primarily of domesticated

ovicaprines. The stable isotope composition of cattle and caprine teeth indicates animals ingested a largely $C_3$ diet that also included some $C_4$ and/or water-stressed $C_3$ vegetation, likely from coastal environments. The flint assemblage includes Canaanean blades indicative of the Late Chalcolithic period and EB I. Taken together, this research proposes that the settlement's edge served as a dump for used artifacts and domestic refuse. Evidence of agricultural activities on the coast is gleaned from seasonal shifts in the carbon and oxygen isotopic composition of incrementally sampled caprine teeth associated with stubble grazing or winter foddering, as well as the presence of large amounts of phytoliths from domesticated cereals (probably emmer wheat), which testify to the engagement of the site's inhabitants with agriculture, likely in the fertile marshland soils found just east of the site. Ceramic petrography, basalt geochemistry, and flint analysis indicate that the site was well connected with inland settlements. Overall, the site is interpreted to have been an EB IA agricultural settlement that also engaged in small-scale trade, which is similar to other EB IA sites known from the southern coastal plain of Israel.

## 1. Introduction

The Early Bronze Age (EB) I in the southern Levant (3800/3700–2800 BCE; Garfinkel, 2014; Goring-Morris and Belfer-Cohen, 2014; Banning, 2019; Greenberg, 2019) is often viewed as a transitional period between the agrarian Neolithic and Chalcolithic village societies and the first Canaanite urban society of the region, which appeared in EB II (Paz, 2002; Milevski et al., 2014; Chesson, 2019). Based on data from inland sites, the EB I population coalesced in very large and densely structured villages (i.e., high population density; site sizes of up to 16 ha), with an agropastoral subsistence economy associated with developed olive and vine horticulture and the appearance of the plow and wheel (de Miroschedji, 2013). Storage methods and exchange networks diversified during this period, and formal trade appeared, associated with the first states (Egypt and Mesopotamia) and involving a land route between Egypt and the southern Levant, as well as a maritime route between Egypt and Byblos (Wengrow, 2006: fig. 7.1; Broodbank, 2013: fig. 7.15). Exchange was optimized overland thanks to the domestication of the donkey (e.g., Arnold et al., 2016). Evidence of maritime exchange of commodities is deduced from a unique find of Nilotic mollusk remains (*Chambardia rubens*) within an EB I jar found underwater at the bay of ʻAtlit (Sharvit et al., 2002). Ample evidence of exchange between the southern Levant and Egypt is found at coastal plain and inland sites in the form of Nile perch remains (Golani, 2013), *serekh*s on ceramics, and certain types of pottery (Yannai and Braun, 2001; Braun, 2014).

While these EB I networks are well known inland and on the inner coastal plain, the picture is less clear along the southern Levant shoreline, where very few EB I settlements—now mostly covered by sand dunes and possibly partially submerged in the sea—have been systematically excavated. The largest shoreline settlements excavated thus far include Ashqelon (explored at three locales: Afridar, Barneʻa, and Marina; Golani, 2013, 2019b) and Palmahim Quarry (Braun, 1992), located in the southern and central shorelines of Israel, respectively. These sites are characterized as being very long and narrow (each several hundreds of meters wide and ca. 1 km long, with an area of ca. 40–70 ha) and include one or two occupation levels. The early phase of the period, EB IA, is characterized by smaller villages that displayed primarily mud-brick architecture and subsisted on agriculture, marine resources (fish, mollusks), and small-scale trade (e.g., Nizzanim, Afridar, and Barneʻa). Most EB IA sites were abandoned, but occupation continued during EB IB at a few sites (e.g., Afridar and Barneʻa), which yielded evidence of larger-scale trade, including donkey remains, basalt bowls, copper from Feynan, and timber from northern areas. A possible maritime component for trade networks, utilizing the Byblos–Egypt line, is therefore postulated for these sites (Gophna and Liphschitz, 1996; Golani, 2013, 2019a, 2022).

Though EB I shoreline sites north of Palmahim have yet to be studied systematically, surveys along the Carmel Coast identified several sites (Olami et al., 2005), with the one we present here, Dor South, seemingly belonging to the phenomenon of the long, narrow sites of the period. During 2018–2020, a survey and three short excavation seasons were conducted at Dor South. The site was extensively damaged by modern activities, and only its northern tip seems to be intact. Because this settlement is unique to the region and period under discussion, the aim of this study is to present basic socioeconomic patterns and resource use on the Carmel Coast during EB IA, as represented at Dor South. We will focus on attributes that enable to evaluate the settlement's nature: its reliance on local coastal as well as nonlocal inland resources and the engagement in trade/exchange.

The approach we take in this study emphasizes material identification and site formation processes on the macro- and microscopic levels, utilizing a battery of macro-and micro-archaeological methods to examine a variety of finds and aspects (stratigraphy, pottery and flint typology, micro-geoarchaeology, phytoliths, faunal stable isotopes, basalt and flint geochemistry, and pottery petrography). Despite major modern disturbance to the site and excavation at its edge, the comprehensiveness of this integrative approach enables to achieve the study's aim successfully.

## 1.1. The study region and site

The site of Dor South was identified in a survey (Olami et al., 2005: Site 145). Its extent—ca. 30 ha in area, with a maximum length of 1 km and a maximum width of 300 m—is noted in the publication, as well as material culture evidence dated to the Early Bronze Age and Chalcolithic period, but the site was not studied further.

Dor South is situated on a sand dune about 1 km south of the Tantura Lagoon, between the modern mouth of the Dalia Stream in the south and a low aeolianite (*kurkar*) outcrop nicknamed "Napoleon Hill" to the north (Fig. 1). The site's western edge lies about 50 m east of the current shoreline; an underwater survey revealed no submerged EB I features west of the land site (Nickelsberg et al., 2022). The region is dominated by shifting sand dunes up to ca. 200 m inland from the shoreline. Where the sand dunes diminish, the region includes shallow outcroppings of *kurkar* associated with flat, dark-brown, marshy clay-rich deposits that serve for agriculture nowadays. It is unknown whether the region was dry or marshy during EB I (a relatively wet period; Rosen, 2007; Bar-Matthews and Ayalon, 2011; Langgut et al., 2016). Galili et al. (2005) have proposed—though without clear-cut evidence—that the sea level at that time was about 2–3 m below the current mean sea level, implying that the shoreline was about 400 m west of the current coastline (Nickelsberg et al., 2022). The site currently lies at an elevation that ranges 1–3 m above mean sea level. It is proposed that coastal marshes became saline during the Chalcolithic period, evidenced by the presence of mollusks that inhabit brackish and hypersaline water bodies, while sand dunes started forming during the Early Bronze Age (Galili et al., 2005). Currently, brackish groundwater level fluctuates between winter (higher) and summer (lower) (R.S.-G., personal observations).

Natural resources in the site's immediate vicinity (within a 3 km radius of the settlement) include *kurkar*, quartz-rich sand, and alluvial/marsh deposits (Fig. 2), which may have been used for construction, pasture, and (dry-farming) agriculture. Yet considering Galili et al.'s (2005) note on the brackish and hypersaline conditions in the marshy parts of the Carmel Coast, livestock pasture and especially dry-farming cultivation would have been highly challenging. From an economic catchment viewpoint (*sensu* Higgs and Vita-Finzi, 1972), this coastal environment and especially shoreline habitation were probably quite difficult for both humans and animals (e.g., malaria infestation; Cropper, 1902), and in fact, Higgs and Vita-Finzi (1972: fig. 4) argued that the Carmel Coast region was not suitable for any type of cultivation and herding. Apart from products of the latter subsistence activities, other, environmental, resources included trees and marsh vegetation, which could have been used for construction, furnishing, basketry, food, and fuel. Wild terrestrial animals could have been consumed, as well as fish and shellfish. Pottery could have been produced locally from marsh deposits or alluvial deposits found along streams. Fresh water could have been obtained from wells; yet these probably became salinized quite often due to sea level rise.

Resources found farther away, between 3 and 10 km from the settlement, include rocks and sediments, flora, and fauna of the western slopes of Mount Carmel. Rock resources include limestone, dolomite, chalk, flint, volcanic tuff, and basalt (Fig. 2). Limestone and dolomite may be of the Lower or Upper Cretaceous (ca. 145–100 Ma and 100–66 Ma, respectively), chalk and flint may be either of the Upper Cretaceous or Paleogene (ca. 66–23 Ma), while volcanics are Upper Cretaceous. These could have served for construction and for pottery, flint tool, and basalt groundstone production. Dry farming, herding, hunting, and gathering may have taken place as well on the slopes of the Carmel ridge.

Despite the inhospitality of the shoreline marshland and sand dune environment, the sea's role in

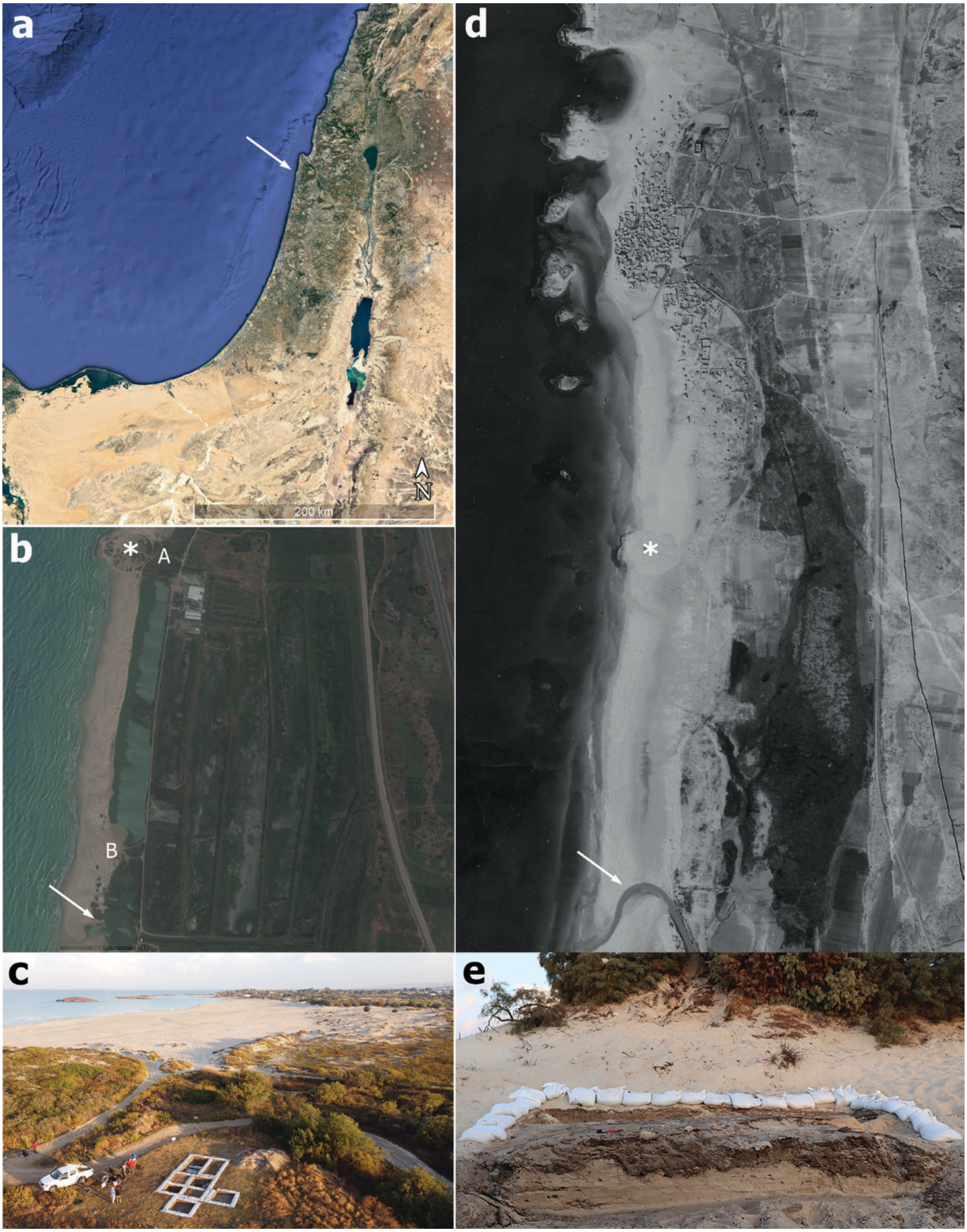


**Figure 1.** (a) Google Earth image of the southeastern Mediterranean; the Carmel Coast is marked with an arrow; (b) Google Earth image from 2018 showing location of Dor South excavation Areas A and B, *kurkar* Napoleon Hill (marked with *), and Dalia Stream outlet (arrow), with elongated artificial fish pond stretching along the coast; (c) oblique aerial photograph from 2020 of excavated area and site's sandy environment (photo by Gerardo Diaz); (d) oblique aerial photograph from 1944 showing region from Tel Dor (top left) to Dalia Stream outlet (arrow) and Napoleon Hill (*); village of Tantura seen north of Napoleon Hill and its cultivated fields to the east; no fish pond construction disturbs coastal strip where Dor South is located (photo obtained from MAPI); (e) excavated section in Area B with brown deposit (bearing artifacts) over loose sand layer, demonstrating site disturbance due to fish pond construction (photo by R. Shahack-Gross).

Mediterranean adaptation and economic risk mitigation grew increasingly significant from the Early Bronze Age onward. Therefore, we may propose that the phenomenon of long and narrow EB I shoreline settlements represents societies deeply engaged with maritime and overland connectivity. This work will provide evidence regarding the geogenic (pottery, basalt, flint) resources used by the site inhabitants, as well as biogenic (fauna and flora) resources indicating dry farming and herding, which together supply information on the economic base of the EB I Dor South settlement.

The site was surveyed and excavated between 2018 and 2020 (Nickelsberg and Shahack-Gross, 2021). Its southern part (Area B) features a 3–15 cm thick clayey deposit bearing artifacts, overlying sand dunes with no architectural remains (Fig. 1e). We interpret this sequence as disturbed deposits resulting from the construction of a fish pond nearby (Fig. 1b). Excavation at the northern part of the site (Area A) revealed stratified deposits with an overall thickness of over 1 m, associated with abundant pottery and flint artifacts. Faunal remains were relatively few, and some basalt groundstone fragments were found as well. The report below presents the results of analyses conducted on sediments, pottery, faunal remains, basalt, and flint.

## 2. Materials and methods

Three short excavation seasons (lasting one, two, and three weeks, respectively) were conducted in 2018–2020. About 75 m$^2$ were excavated using a 5 × 5 m grid, with each excavation square measuring 4 × 4 m, leaving a 1 m wide baulk between excavated squares (Fig. 1c). The baulks enabled to control the stratigraphic units, and their sections served for micro-geoarchaeological sampling of excavation profiles. The squares were excavated to different depths, ranging from merely 30 cm to as much as 1.60 m below the surface. Five deep soundings (in Squares A1, B3, C2, D2 NE, and D2 SW) reached sterile bedrock (yellow sand and/or calcite-indurated

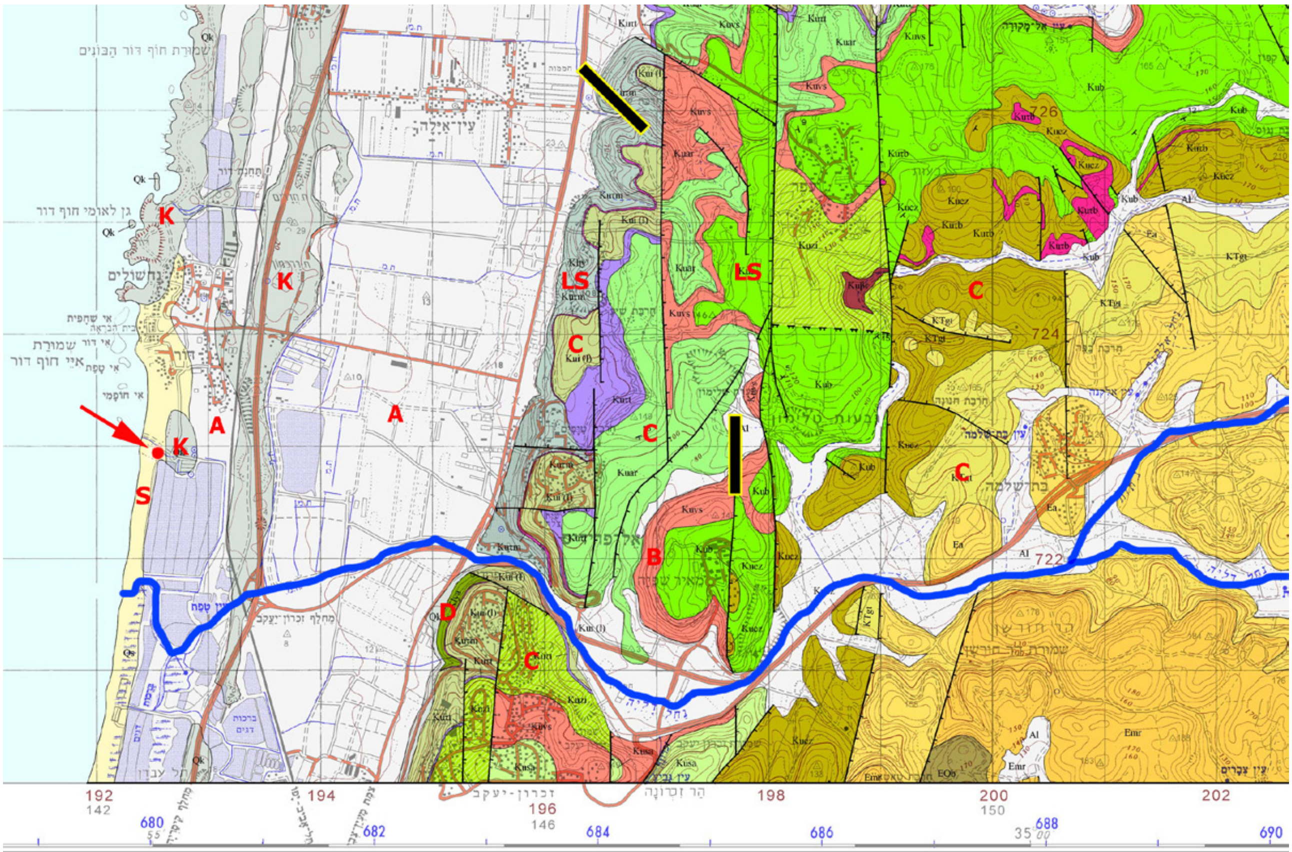


**Figure 2.** Geological map of study region (Segev and Sass, 2009; courtesy of the Geological Survey of Israel) showing Area A (marked by red point and arrow) and Dalia Stream (marked in blue); short black lines mark 5 km distance from the site to the east and northeast; letters indicate rock types, soils, and sediments: S = sand; K = *kurkar*; A = alluvial and marsh deposits; LS = limestone; D = dolomite; C = chalk (all chalk formations include flint nodules); B = basalt.

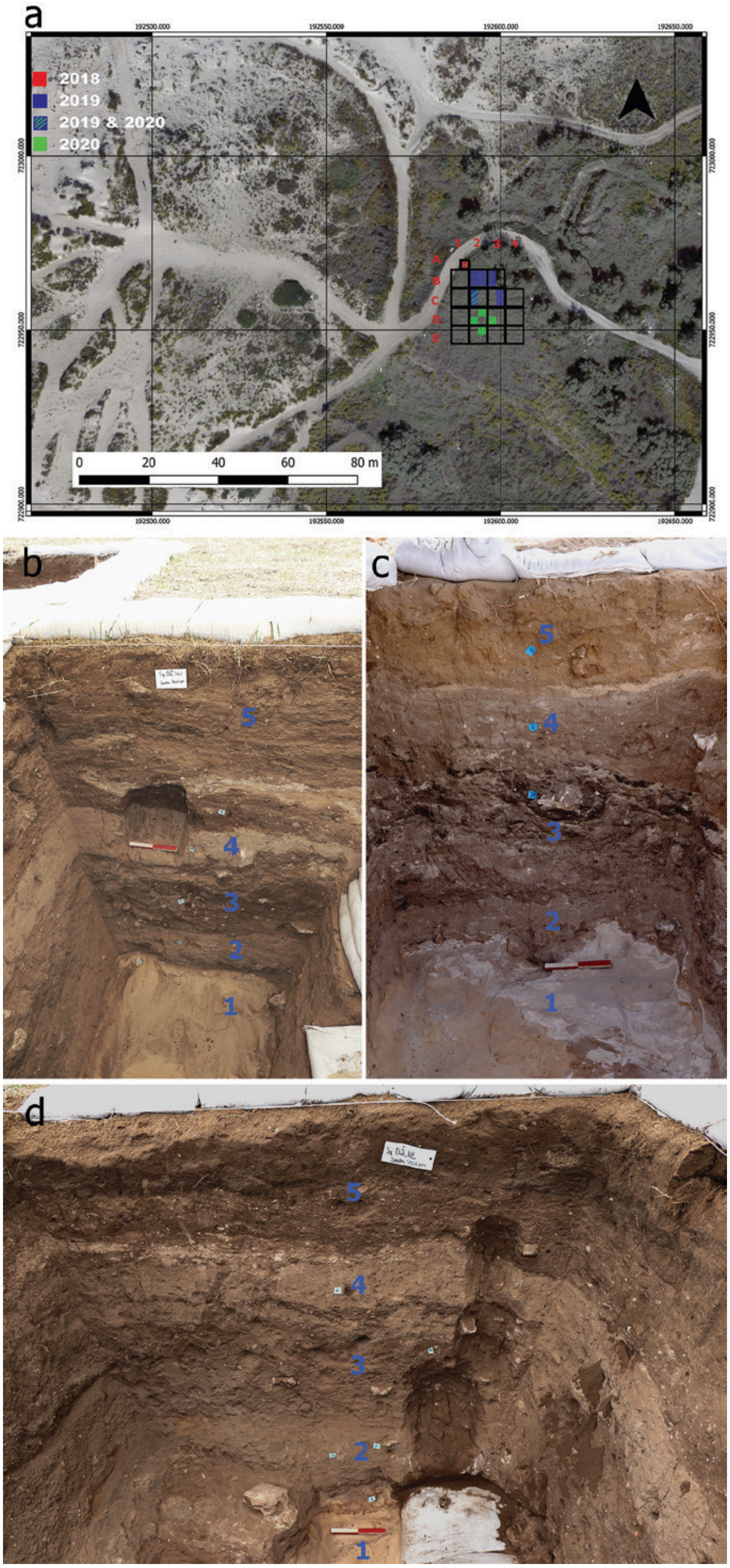


**Figure 3.** Site grid and stratigraphy: (a) 5 × 5 m site grid; colors indicate squares excavated in various seasons; (b) excavation profile in Square D2 SW (south section, ca. 1.30 m from surface to sterile deposits); (c) excavation profile in Square A1 (east section, ca. 1.20 m from surface to sterile deposits); (d) excavation profile in Square D2 NE (south section, ca. 1.55 m from surface to sterile deposits). Note the same stratigraphic units across the site, from bottom to top: Layer 1: sterile sand or calcite-indurated sand; Layer 2: fine-grained gray deposit; Layer 3: dark-brown deposit including rocks; Layer 4: fine-grained gray deposit; Layer 5: laminated topsoil deposits. Scale bar in all profiles is 20 cm long. Blue tags attached to profiles indicate position of bulk sample collection, while rectangular depressions in the profiles are where sediment monoliths for micromorphological analysis have been extracted (photos by R. Shahack-Gross).

sterile sand; Layer 1 in Fig. 3b–d) at depths ranging between 1.20 and 1.55 m below the surface.

Finds were primarily hand collected, while coarse (1 cm) and fine (0.5 and 1.0 mm) sieving was conducted occasionally, according to field observations and features. Chronology was determined solely on the typological study of the retrieved pottery, as no samples were found that were suitable for radiocarbon dating. The overall ceramic assemblage amounts to ca. 400 typologically identifiable items, of which 20 representative sherds from undisturbed loci were analyzed. They have parallels at distant sites, such as Ashqelon Afridar and Barne'a (Golani, 2008; Golani and Pasternack, 2020; Golani and Talis, 2022) and Fazael 4 (Bar et al., 2021), while the closest similarities were found at 'En Esur (Yannai, 2006).

Deposits were described using geoarchaeological criteria (e.g., Karkanas and Goldberg, 2018). Sediments were collected as bulk (loose) and monolith (intact, oriented, portions of deposits, mostly around contacts of depositional units) samples. There are 101 bulk samples, which served for all bulk analyses, and 11 monoliths, which served for the micromorphological analysis. Bulk mineralogy, as well as quantification of anthropogenic micro-remains—phytoliths, dung spherulites, and ash pseudomorphs—were carried out on the bulk sediment samples. Mineralogy was determined via Fourier transform infrared (FTIR) analysis using a Thermo Scientific Nicolet iS5 spectrometer and employing the KBr method (details in Ogloblin Ramirez et al., 2020). Evidence of clay heating was determined using criteria in Berna et al. (2007).

Phytolith extraction and quantification followed the procedure of Katz et al. (2010), while dung spherulite and ash pseudomorph extraction and quantification followed the procedure of Gur-Arieh et al. (2013). Phytolith morphologies were studied at a 400× magnification using an Olympus BX53 Polarizing Microscope. Morphology identification followed the international code for phytolith nomenclature (Madella et al., 2005; International Committee for Phytolith Taxonomy [ICPT], 2019). Six sediment samples were studied from Layers 2–4, two per layer, to ascertain reproducibility. Phytolith morphologies were counted until a minimum number of 200 phytoliths was reached, and the single cells in silica skeletons, which were noted separately, were added to the total number of morphotypes only after reaching 200, in order to avoid a morphological bias.

Sediment monoliths were impregnated with polyester resin and prepared as 30 µm thin sections after curing for micromorphological analysis. The descriptions follow the international nomenclature (Stoops, 2003).

Faunal analysis focused on taxonomic identification. Taphonomic analysis was not conducted due to the small sample size of only 28 identifiable specimens.

Bone and tooth specimens were sampled for stable carbon ($\delta^{13}C$) and nitrogen ($\delta^{15}N$) isotope analysis of collagen and for carbon ($\delta^{13}C$) and oxygen ($\delta^{18}O$) isotope analysis of enamel bioapatite, respectively. Bone chunks were demineralized in 0.5M EDTA, rinsed 15 times in ultrapure distilled water with an overnight soak before the seventh rinse, and lyophilized (Tuross et al., 1989). Molar teeth were sequentially drilled using a Dremel diamond-tipped drill. The enamel powder extracted from each of the samples was reacted with a buffer solution containing 0.1M acetic acid for four hours to remove diagenetic carbonates (Balasse et al., 2003), rinsed five times with distilled water, and then freeze-dried. Sampled powders were not treated with NaClO before the acetic acid step, to avoid recrystallization of the hydroxyapatite lattice, which is known to alter *in vivo* oxygen and, to a lesser extent, carbon isotope values in bioapatite. Faunal collagens were analyzed for $\delta^{13}C$, $\delta^{15}N$, %C, and %N on a vario PYRO cube elemental analyzer coupled to an isoprime visION mass spectrometer in continuous flow mode at the Archaeology Stable Isotope Laboratory (ASIL), University of Kiel. The treated bioapatite powders were measured for $\delta^{13}C$ and $\delta^{18}O$ with a KIEL IV Carbonate Device interfaced to a Finnigan MAT 253 isotope ratio mass spectrometer at the Leibniz Laboratory for Radiometric Dating and Isotope Research, University of Kiel.

Basalt geochemistry was conducted on eight archaeological specimens and seven geological references. Details of materials and analytical methods are provided in Appendix A.

The lithic assemblage included 1415 flint items larger than 1.5 cm, with the exception of tools and tool fragments. The analysis focused on *chaîn opératoire* stages (Perlès, 1987; Sellet, 1993) and techno-typology (Rosen, 1997; Inizan et al., 1999). The tools were classified mainly according to Rosen's (1997) typology, with some slight modifications. Each piece was recorded by type of blank (blade, bladelet, flake, primary element, etc.) and core or tool type. Primary elements are defined as blanks with more than 30% cortex, while the distinction between blades and bladelets follows Tixier (1963), with items ≥ 12 mm wide defined as blades.

# 3. Results

## 3.1. Chronology

The majority of the pottery is associated with EB IA. Some sherds are indicative of EB IB, and others date to the Chalcolithic period and possibly even the early Pottery Neolithic (Fig. 4). Appendix B presents the full description of the pottery assemblage.

## 3.2. Stratigraphy and characterization of the deposits

As the excavated portion of the site (Fig. 3a) yielded no architectural features (walls, floors, installations), the study focused on deposits. Observations across the profiles exposed in baulk sections revealed a repetitive pattern consisting of five layers, presented here from bottom to top:

**Layer 1**: Archaeologically sterile, loose, yellow sand or white calcite-indurated sand; the latter appears as irregular patches (Fig. 3b–d). This layer was reached at depths of approximately 120–155 cm below surface (188–192 cm above mean sea level).

All layers above it include pottery, stones, flint items, basalt groundstone fragments, and faunal remains. Macroscopic charred botanical remains are absent.

**Layer 2**: A ca. 10–20 cm thick very hard and fine-grained gray deposit.

**Layer 3**: A ca. 30–50 cm thick hard dark-brown deposit, often containing stones.

**Layer 4**: A ca. 10–30 cm thick hard and fine-grained gray deposit.

**Layer 5**: A ca. 30–60 cm thick series of laminated deposits, including stringers of yellow sand and many circular to oblong rodent burrows.

Mineralogically, all sediment samples are dominated by quartz (from coastal sand) and include also clay and calcite. Heated clay was detected only in the deepest occupation deposit, Layer 2, in Square D2 NE (Table 1).

Economic micro-remains (i.e., cereal phytoliths, dung spherulites, and wood ash crystals) quantified across the excavation area and stratigraphic sequence are dominated by phytoliths. The highest phytolith concentrations were found in samples of Layers 2 and 4, both fine-grained and gray colored (Table 1). Phytolith concentrations therefore correlate with the macrostratigraphic division.

### *3.2.1. Phytolith morphotype analysis*

This analysis, detailed in Appendix C, shows a well-preserved phytolith assemblage, based on the presence of less than 8% weathered and melted phytoliths and a high percentage (15–28%) of multicellular structures. The phytolith assemblages in the six sediment samples are dominated by monocotyledonous morphotypes (81–93%), of which more than a third originate in inflorescences (34–45%). The rest of the morphotypes originate in dicotyledonous wood and bark (3–13%),

**Table 1.** Results of bulk micro-geoarchaeological analyses according to macro-stratigraphy

| **Layer** | **No. of samples analyzed** | Mineralogy **(decreasing abundance)** | **Phytolith concentration range (millions/1g sediment)** | **Dung spherulite concentration range (millions/1g sediment)** | **Ash pseudomorph concentration range (millions/1g sediment)** |
|---|---|---|---|---|---|
| 1 | 9 | Quartz, calcite | 0–1 | 0 | 0 |
| 2 | 6 | Quartz, calcite, clay | 15–36 | 0 | 0–1 |
| 3 | 17 | Quartz, clay, calcite | 2–20 | 0 | 0 |
| 4 | 9 | Quartz, calcite, clay, opal | 7–33 | 0 | 0 |
| 5 | 8 | Quartz, clay, calcite | 1–19 | 0 | 0 |

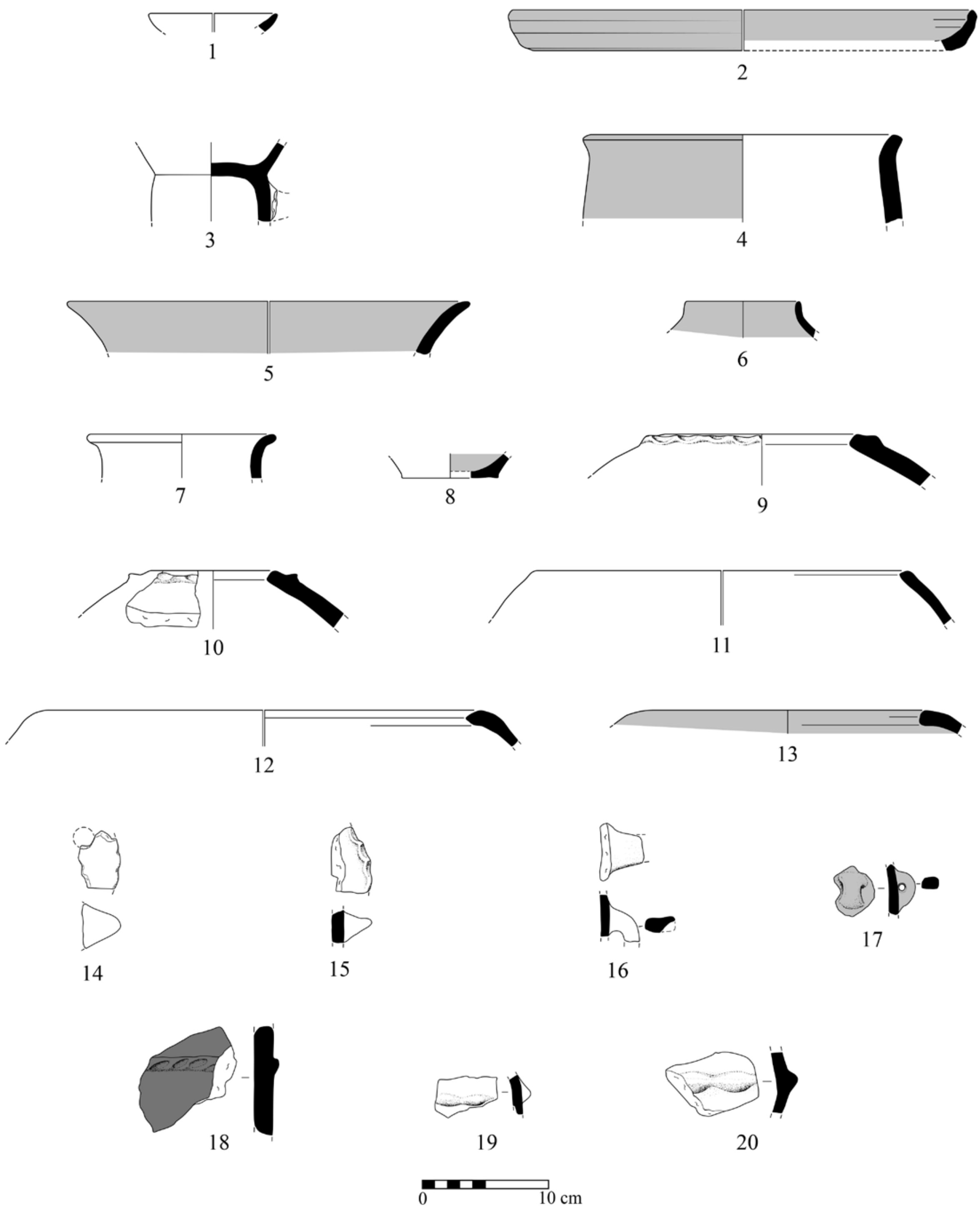


**Figure 4.** The pottery assemblage, including bowls (1–3), storage jars (4–8), holemouth jars (9–13), handles (14–18), and GBW (19–20) (drawings by Sapir Haad); see Appendix B.

dicotyledonous leaves (0–2%), and Cyperaceae (2–4%, only in Layer 2). $C_3$ grass phytoliths form 65–90% of the assemblage, and the rest of the grass phytoliths originate in $C_4$ grasses. Notably, $C_4$ grasses are more abundant in Layers 2 and 4 than in Layer 3. In five of the six samples analyzed, dendritic phytoliths form 15–20% of the morphotype assemblage.

Taken together, Layer 2 (lower gray) is characterized by high phytolith concentrations and a $C_3$ grass assemblage with more than 15% dendritic phytoliths, as well as $C_4$ and Cyperaceae phytoliths; Layer 3 (middle, brown) is characterized by low phytolith concentrations and dominated by $C_3$ grass phytoliths with lower percentage of dendritics; and Layer 4 (upper gray) is characterized by high phytolith concentrations, a $C_3$ grass assemblage with more than 15% dendritic phytoliths, and $C_4$ grasses.

### 3.2.2. Micromorphology

Sediment micromorphology supports and amplifies the macroscopic observations on the five stratigraphic layers. All layers are composed of medium-sand-sized quartz grains typical of the Carmel Coast (Fig. 5a–d). Apart from the abundant quartz grains, the layers contain the following:

**Layer 1** contains marine shell and sea urchin spine fragments in the medium-sand size category, typical of coastal dunes along the Carmel Coast. These grains are cemented by calcite, giving the appearance of an incipient formation of *kurkar* (Fig. 5d). No micro-artifacts occur in this deposit.

**Layer 2** includes a clay and calcite matrix, as well as sparse rounded soil aggregates, sand-sized bone fragments, micro-charcoal, and wood ash (Fig. 5c). Additionally, domains of calcite cementation occur occasionally, appearing as pedogenic nodules.

**Layer 3** is dominated by quartz sand grains with little clay matrix and almost devoid of micro-artifacts (Fig. 5b).

**Layer 4** is the richest in macro- and micro-artifacts. It includes abundant flint items (Fig. 5a), shells, bones, soil aggregates (Fig. 5e, f), and an ashy calcitic matrix with micro-charcoal and grass phytoliths (Fig. 5g). This deposit shows evidence of partial dissolution of carbonate components, such as shells (Fig. 5f), and their re-precipitation either as pendants beneath artifacts or as patches of cemented matrix (Fig. 5a). Except for flint, all micro-artifacts are rounded, indicating rolling and/or trampling, while soil aggregates are mostly medium-sand sized, suggesting they may have been rolled and deposited by wind.

**Layer 5** is mixed topsoil; therefore, its micromorphological features are not archaeologically illuminating, and it will not be discussed further.

Overall, depositional and postdepositional processes include aeolian coastal dune formation and its cementation (Layer 1), initial anthropogenic activity typified by sparse micro-artifacts in a coastal dune environment that underwent incipient pedogenesis (Layer 2), abundant degraded mud-brick material practically devoid of micro-artifacts (Layer 3), and an anthropogenic deposit abundant with varied micro-artifacts in which carbonate-containing artifacts (shells, wood ash, bones) were partially dissolved, while the ensuing solution re-precipitated as calcite pendants and cemented portions of the deposit's matrix (Layer 4).

## 3.3. Faunal analyses

The faunal remains comprise 28 identified specimens (Table 2). Density mediated attrition is evident in the high frequency of tooth and shaft fragments among them. The most common animal species are caprines, followed by cattle and pigs.

Altogether, collagen preservation was very poor in faunal bone specimens recovered at Dor South, with collagen successfully extracted from only one caprine

**Table 2.** Identified faunal remains at Dor South

| Taxonomic group | No. of identified specimens |
|---|---|
| Caprine | 11 |
| Cattle | 3 |
| Pig | 3 |
| Fallow deer | 3 |
| Equid | 2 |
| Dog | 1 |
| Turtle | 1 |
| Fish | 1 |
| Rodent | 1 |
| Large mammal | 1 |
| Medium mammal | 1 |

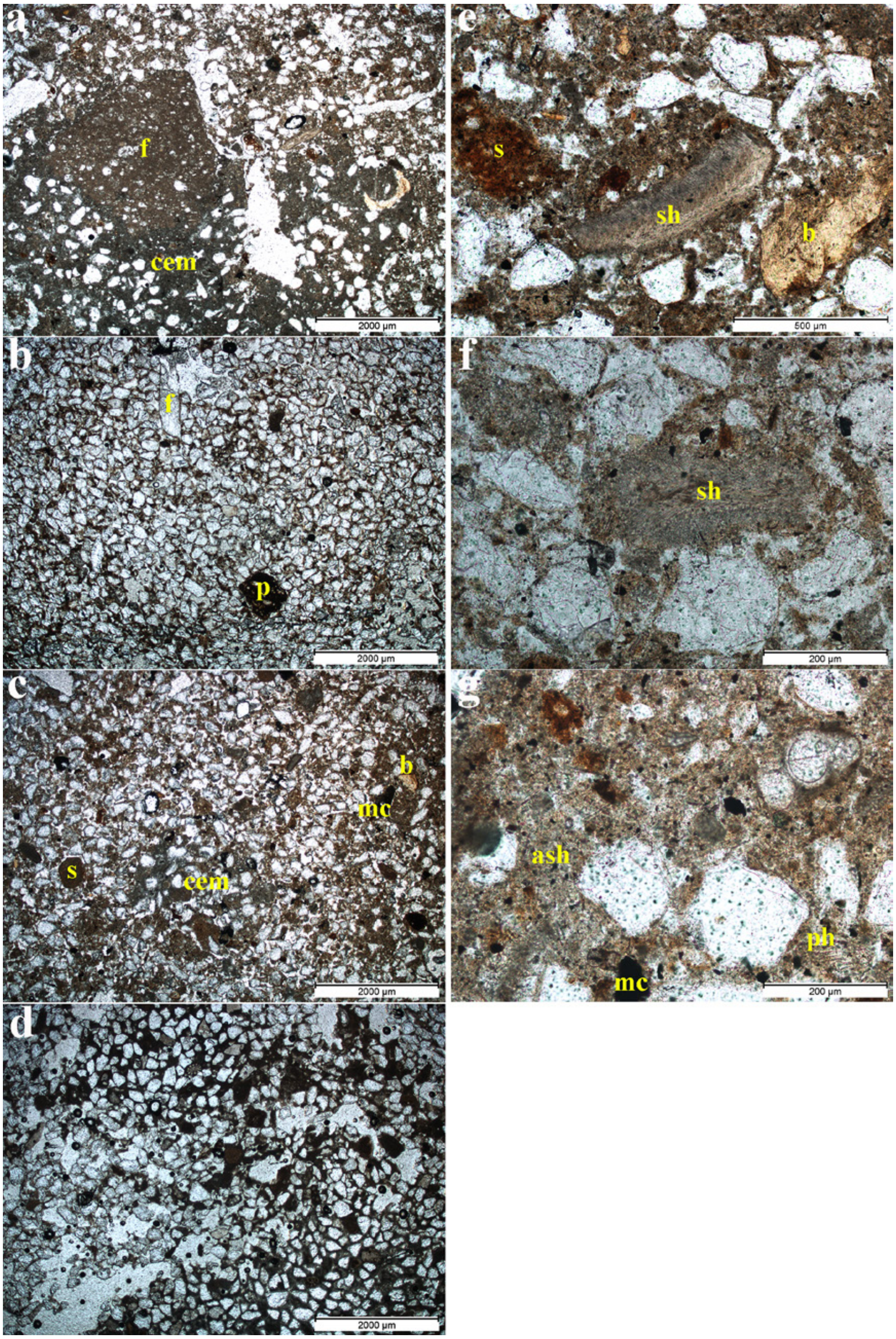


**Figure 5.** Micromorphology. All images are in plane polarized light. Context details for the position of the blocks used to create this figure are presented in Appendix F.

Images on the left column show the characteristics of Layers 1–4: (a) Layer 4, Block DS20A-4-1: sandy gray deposit including a flint particle (f) with silicified foraminifera typical of the nearby Eocene Adulam Formation (see Fig. 2). The grayish matrix is partially cemented (cem), and a pendant is noted below the flint particle. Brown rounded particles are rolled soil aggregates. This deposit includes large amounts of anthropogenic materials (see images 5e–g). (b) Layer 3, Block DS18A-2-4: dark-brown sandy deposit, including occasional flint (f) and pottery (p) fragments. (c) Layer 2, Block DS20A-3-3: sandy grayish-brown deposit that includes occasional anthropogenic materials (bone fragments) (b) and micro-charcoal (mc), as well as rounded soil aggregates (s) and cemented patches (cem). (d) Layer 1, Block DS20A-5-3: white cemented sandy deposit that includes fragments of shells and sea urchin spines, indicating this is a lithified coastal dune (i.e., incipient formation of *kurkar*). Images in the right column are close-ups on features characteristic to Layer 4, from Block DS20A-4-1: (e) rounded fragments of soil (s), marine shell (sh) and bone (b) in an ashy matrix containing quartz sand; (f) a shell fragment (sh) showing dissolved edges; (g) ashy matrix (ash) with microcharcoal (mc) and grass phytoliths (ph) (photos by R. Shahack-Gross).

specimen. This specimen yielded well-preserved collagen that passed established quality control criteria (%C = 42, %N = 14.9, atomic C/N ratio = 3.3) and a $\delta^{13}C$ value of –21.5‰ and a $\delta^{15}N$ value of 5.1‰. Taking into account a ca. 5‰ diet-collagen offset ($\delta^{13}C_{diet}$ = –26.5‰), this individual animal consumed $C_3$ vegetation with no input from $C_4$ or $^{13}C$-enriched $C_3$ flora. The relatively low nitrogen isotope value suggests this individual grazed extensively on either forage or pastures, supporting a low stocking rate. However, additional nitrogen isotopic data from multiple taxa are required to establish the distribution of nitrogen isotopes at the floral base of the food web.

The carbon isotopic composition of enamel carbonates from sequentially sampled faunal teeth indicates seasonal variation in animal dietary intake. Cattle (n = 2) exhibited a particularly wide variation in $\delta^{13}C_{diet}$ values (14.1‰ diet-tissue offset) ranging from ca. –24‰ to ca. –16.5‰. The diet of Individual 10470, which was seasonally focused on a mixed $C_3$/$C_4$ diet during late winter/early spring, shifted to $^{13}C$-enriched $C_4$ plants, probably during late summer/early autumn, as indicated by high $\delta^{13}C$ values expressed after $\delta^{8}O_{max}$ values within the sequence, and later shifted again to a more mixed $C_3$/$C_4$ diet (Fig. 6). Sedges were one readily available and abundant source of $C_4$ plants in the Dor South area. Specimen 10472 yielded considerably lower $\delta^{13}C_{diet}$ values, ranging from ca. –24‰ to ca. –22‰, indicating this individual ingested a $C_3$ diet during one portion of the year and a $C_3$-based diet with some $C_4$- and/or $^{13}C$-enriched $C_3$ contribution later in the year; the absence of a clear sinusoidal pattern in the oxygen isotopes of this individual presents difficulties in establishing the seasons of dietary change. The three caprine specimens yielded $\delta^{13}C_{diet}$ values ranging from ca. –22‰ to –26‰, indicating their diets comprised mainly $C_3$ forage, perhaps mixed browse and $^{13}C$-enriched grasses. One specimen (11937) yielded a (summer) seasonal low $\delta^{13}C_{diet}$ value of –26‰; this individual may have browsed in a lightly wooded landscape or ingested very well-watered graze during the warmer months. Higher dietary carbon isotope values reaching –22‰ in this individual correspond with low $\delta^{18}O$ values, indicating a seasonal contribution of $^{13}C$-enriched graze from water-stressed flora, possibly growing under saline conditions, which promote water stress, during the cooler months. All caprines yielded intra-tooth isotope patterns where high summer season $\delta^{18}O$ maxima values correspond with low $\delta^{13}C$ values. This pattern suggests animals grazed on $^{13}C$-depleted forage grown under well-watered conditions during the summer months and foddered with a $^{13}C$-enriched, likely stored, food source in the winter season.

### 3.4. Basalt geochemistry

The assemblage of basalt vessels from Dor South includes four bowls, three grinding stones, and one spindle whorl (Appendix A). All are typologically consistent with EB I.

The chemical compositions of the studied geological and archaeological samples are presented in Appendix A, Table A.4. A total alkali to silica (TAS) diagram (Le Maitre et al., 1989) shows that geological references vary across alkaline basalts and highly alkaline basanite with four samples below the subalkaline basalt line (Fig. 7). The archaeological samples belong primarily to subalkaline and alkaline basalts, with one exception, item DS-22, which falls in the region of basanite (Fig. 7). The compositions in the TAS diagram of our reference samples correspond well with the compositions obtained for basalts sampled in nearby locations (specifically samples from the Miocene [ca. 23–5 Ma] outcrops at Giv'at Kipod and Midrach Oz; Gluhak and

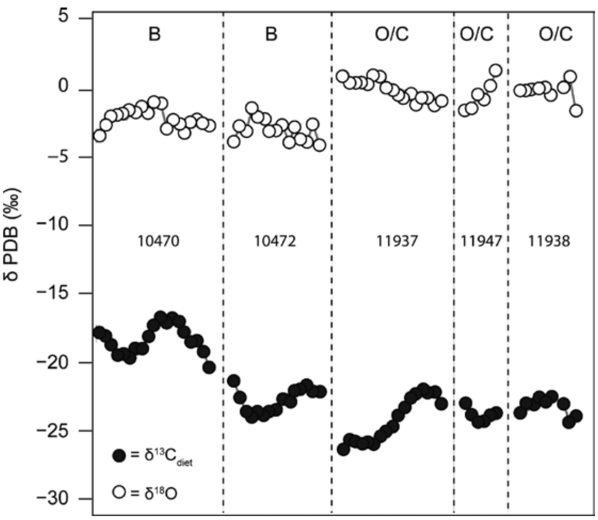


**Figure 6.** Dietary carbon ($\delta^{13}C$) isotope values (black circles; 14.1‰ diet-bioapatite offset) and oxygen ($\delta^{18}O$) isotopes (circle outlines) for incrementally sampled molar teeth. From left to right: Dor South cattle (10470, 10472) and ovicaprines (11937, 11947, 11938). The left-most data point for each sequence is the nearest to the tooth occlusal surface, while the right-most data point is the nearest to the enamel-root junction (prepared by C. Makarewicz).

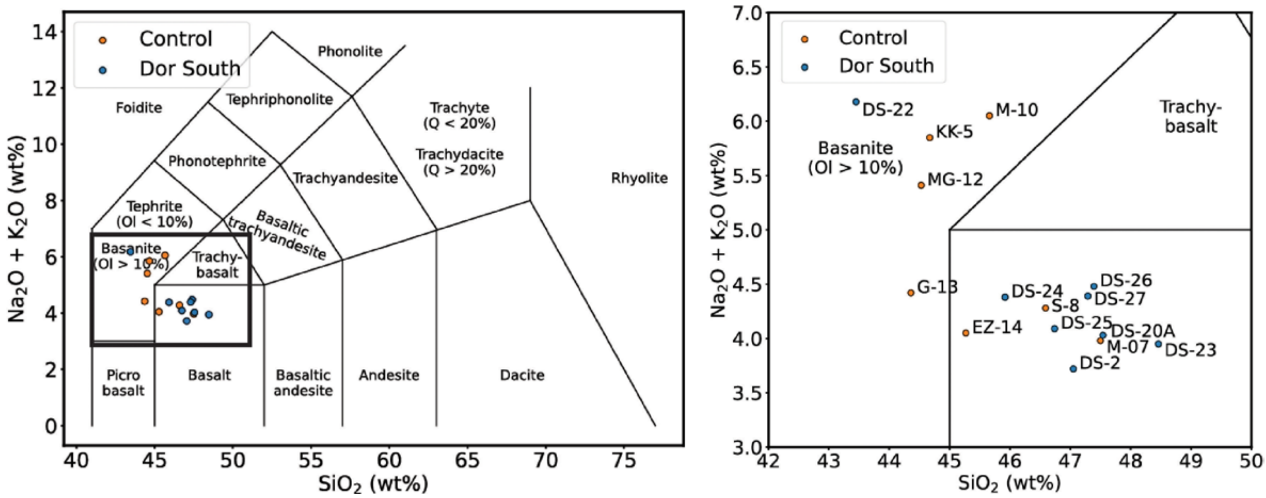


**Figure 7.** Archeological and geological basalts analyzed in this study, plotted on a TAS diagram (prepared by I. Patania).

Rosenberg, 2013). The seven clustered archaeological samples plot together with our reference samples collected at Midrach Oz and Shefeya (Fig. 7).

Elemental bi-plots of major oxides ($SiO_2$ vs. MgO, $P_2O_5$, and $TiO_2$) reveal a similar pattern: seven of the eight archaeological items plot together with references from Midrach Oz and Shefeya, while sample DS-22 stands alone (Fig. 8a–c). A bi-plot of trace elements (for example, $SiO_2$ vs. La; Fig. 8d) reinforces this pattern. Note that sample DS-22 is exceptionally enriched in Ni, Cr, and Mo (Appendix A: Table A.4).

### 3.5. The flint assemblage

The flint assemblage from Dor South (Fig. 9) includes items from a variety of raw material sources, as determined by their color and texture. All of the knapping stages are represented in the assemblage, reflecting *in situ* knapping, beginning with preparation of the core, through the production of blanks, to retouching and use, and finally discarding. The assemblage is dominated by flakes (n = 551; 46.4%; Appendix D), followed by blades and bladelets (n = 103; 8.7%; Appendix D). Cores with a single striking platform are the most common (n = 46; 38% of the total core assemblage). Tools (n = 139) include retouched pieces (n = 54; 38.8% of the tool assemblage; Appendix D), notched and denticulated tools (n = 21; 15.1%), and perforators (n = 15; 10.8%). Eleven Canaanean blades were found: eight of them were used as tools, with four exhibiting sheen, suggesting they were used as sickle blades.

### 3.6. Other items

Three stone items of special interest were found in Layers 3 and 4 (Appendix E), and analyzed using FTIR spectroscopy: a basalt weight (B20A-10-4), a spindle whorl made of an unidentified silicate rock that was polished (B20A-24-3), and a fragment of what was possibly another spindle whorl, made of hematite (B20A-41-3).

## 4. Discussion

The site of Dor South, an EB IA coastal settlement (at least in its northernmost part), was uniquely excavated employing a micro-geoarchaeological approach and methodology. While there have been past excavations at coastal sites dating to this period, none utilized this approach, which contributes considerably to understanding subsistence economy.

Pottery, flint, groundstone tool, and animal bone assemblages are all similar to those from EB I sites in the south, particularly locales in Ashqelon (Golani, 2008, 2022). The ceramic assemblage recovered during the excavation of Dor South is small yet represents the expected pottery from an EB IA village. Items from the lower levels may belong to Pottery Neolithic and/or Chalcolithic phases that preceded the EB I habitation. The excavated area yielded no architectural remains; therefore, we hypothesize that the excavation unearthed the settlement's edge or a very large courtyard/open space within the settlement.

Radiometric dating of the site was not conducted due to the absence of a statistically valid sample of charred botanical remains. The paucity of charred remains is probably the result of site formation processes.

## 4.1. Site formation processes

The site of Dor South formed on a coastal dune, which, as typical of the Carmel Coast, is composed of sand-sized grains of quartz and mollusk shells—referred to in this work as Layer 1. The uppermost part of this unit underwent cementation by calcite, a process similar to the formation of *kurkar*. Based on the date of the earliest remains, this process occurred during the Holocene—that is, Layer 1 belongs to the latest *kurkar* formation in the southern Levantine coast, the Tel Aviv *kurkar* formation (Porat et al., 2004). The earliest human activity, resulting in the formation of Layer 2, includes evidence of wood ash and charcoal. The calcitic wood ash, easily soluble in a sandy matrix, may have contributed to the cementation of the upper part of Layer 1. The anthropogenic deposit includes evidence of incipient pedogenesis, which implies that there was a period of no habitation and stability of the Layer 2 deposit, prior to the formation of the anthropogenic Layers 3 and 4. Layer 3 is interpreted to be composed predominantly of disintegrated mud constructions (mud bricks, pisé, or the like; note that stone architecture has not been found during excavations), as it is not as rich in anthropogenic remains as Layer 4 and contains more clay in its matrix. Layer 4 is the richest in anthropogenic macro- and microscopic remains. It includes very high concentrations of phytoliths, as well as evidence of the dissolution of carbonate-containing materials (ash, bones) and re-precipitation of calcite as pendants below pottery, flint, and basalt artifacts and also as infilling of cracks within these artifacts. The uppermost Layer 5 is highly disturbed topsoil.

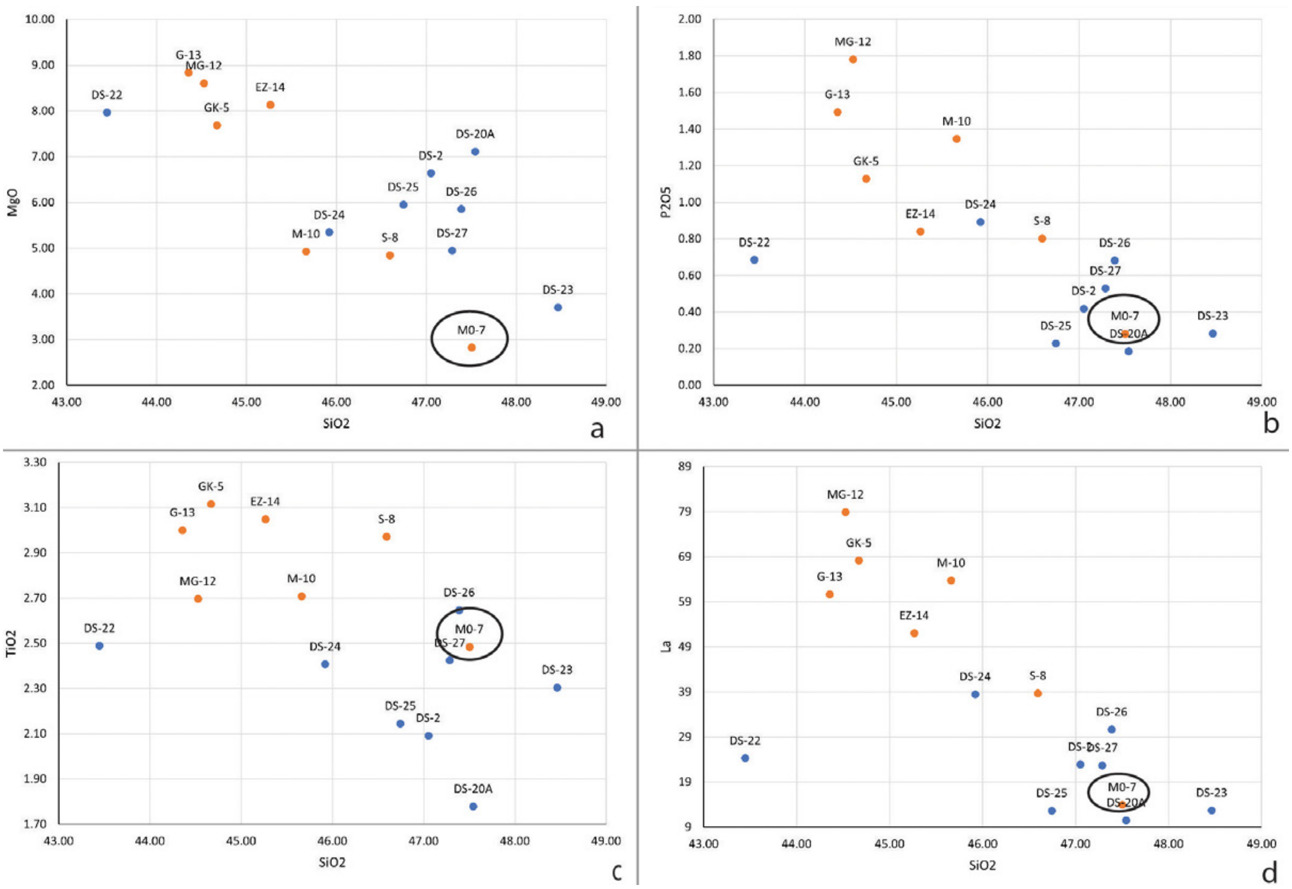


**Figure 8.** Major oxides and the rare earth element La vs. silica concentrations showing clustering of most archaeological items with MO-7 geological sample (circled), collected from the Midrach Oz area. Note also archaeological sample DS-22 occurring outside of the archaeological cluster. Blue dots: archaeological samples; orange dots: geological samples (prepared by I. Patania).


**Figure 9.** Tools from the flint assemblage: (1–3) Canaanean sickle blades; (4) sickle blade; (5–6) perforators; (7) adze (prepared by G. Bermatov-Paz). For details, see Appendix D.

Notably, Layers 2 and 4, although separated by a deposit of degraded mud construction (Layer 3), do not differ in their ceramic and lithic inclusions. The degraded mud in Layer 3 may have originated in disintegrating structures and thus reflects a period of abandonment that was short enough for the material culture remains in the preceding and later occupation phases not to differ significantly. Alternatively, it may reflect dumped mud-brick material as part of dismantling or refurbishing of settlement structures, rather than abandonment. In any case, the evidence of construction with mud rather than elaborate stone walls accords with similar observations in EB IA settlements in the southern coastal plain (Ashqelon Afridar, Barne'a, and Marina; Golani, 2008, 2019a, 2022).

Evidence of bioturbation is abundant, in the form of both macroscopic krotovinas and microscopic passage features, indicating animal burrowing within the soft sandy deposits. Bioturbation probably involves also plant roots, while the upper topsoil may have been disturbed by premodern plowing and modern construction activities (such as the creation of the pond south of the excavated area). The extensive bioturbation may have contributed to fragmentation of macroscopic charred materials, as micro-charcoal is evident in thin sections of the anthropogenic layers.

The extensive postdepositional dissolution of carbonate-containing materials probably relates to the porous nature of the sandy occupation deposits, in which rainwater can easily permeate. If the upper anthropogenic Layer 4 included dung spherulites and ash pseudomorphs, they probably did not survive the ca. 5000 years of water percolation in this coastal dune environment. The postdepositional processes have implications for the preservation of economic macro- and micro-remains, as detailed below.

## 4.2. Reconstructed economic activities

Economic activities at Dor South are reconstructed as follows:

### *4.2.1 Food procurement*

**(A) Fauna**: The faunal assemblage is dominated by ovicaprines and includes also cattle, pigs, equids, a dog, and wild animals. This composition is also found at Ashqelon Barne'a (Zidane and Bar-Oz, 2022). Despite the small sample size, one could get a glimpse of a faunal economy typical of wetland regions: a relatively high percentage of cattle and pigs—animals that have high water requirements—and some hunting. The animal bone finds, compared with other sites, show a Mediterranean economy.

Focusing on domesticated animals, the stable isotope data from the two cattle and three ovicaprine teeth indicate that caprine seasonally ingested primarily $C_3$ vegetation with a small contribution of $C_4$ and/or $^{13}C$-enriched $C_3$ vegetation at other times of the year. This is echoed by the high concentrations of grass phytoliths, interpreted to originate in degraded livestock (primarily cattle and ovicaprine) dung. While phytolith morphotypes are primarily of $C_3$ grasses, they also show minor amounts of $C_4$ grasses and sedges. $C_4$ grasses and certain sedges are found on the coast, having adapted to sandy soils and saline water conditions (Danin and Fragman-Sapir, 2009).

It is noted that mollusk shells other than the prevalent *Glycymeris* sp. (found naturally along the Israeli beach and thus occurring at coastal sites either unrelated to human activities or as a construction material; e.g., Ktalav, 2022) were scarce, while fish bones were not found despite fine sieving of sediments from certain loci. The latter may have either dissolved, as did carbonatic elements (e.g., ash and spherulites) and evidence of dissolution on mammal bones, or they may have not been deposited in the excavated area in the first place. These are somewhat unexpected scarcities for a seaside settlement; however, considering the small scale of the excavation (75 $m^2$), in comparison with other EB IA sites, where much larger areas have been exposed (e.g., ca. 30,000 $m^2$ at Ashqelon Barne'a), this scarcity may be explained in terms of probability of finds per excavation area.

**(B) Agriculture**: Plant remains in the form of phytoliths are abundant. The phytolith assemblage is dominated by grasses and includes a high proportion of inflorescence phytoliths, indicating that plant material was consumed during spring and summer. Moreover, the inflorescence phytolith assemblage includes a high proportion of dendritic long cell phytoliths, indicating the consumption of domesticated wheat (based on data presented in Albert et al., 2008). This evidence, together with the presence of sickle blades, suggests local growth of wheat, further indicating that Dor South was a permanent settlement engaged in cereal cultivation. The presence of grinding tools suggests that cereals were processed.

Overall, evidence from EB IA Dor South points to a Mediterranean village economy based on cereal cultivation and its processing, as well as herding. Year-round grazing was conducted in a Mediterranean landscape close to water sources (sedges), and the livestock diet was supplemented by agricultural by-products. Data from other EB IA coastal sites accord with this conclusion (e.g., Gophna, 1997; Golani, 2022).

### *4.2.2. Domestic activities*

The pottery assemblage, the groundstone tools, and the lithic assemblage represent the expected toolkit for household activities, including food preparation, cooking, food consumption, woodworking, and storage. The pottery assemblage is dominated by storage jars, including holemouth jars, indicating the accumulation of surplus. Some of the latter have soot marks, indicating that these may have been used for cooking. Other pottery vessels, such as bowls, were used for consumption. While Gray Burnished Ware (GBW) vessels have been considered prestigious goods, they have also been linked to food consumption, perhaps by the elite (Greenberg, 2019: 36). Some GBW bowls documented at Ashqelon Barne'a were produced locally, while others were imported from the Galilee (Cohen-Weinberger, 2022). The groundstone tools from the site are dominated by small bowls and grinding stones, which were used for grinding agricultural products, possibly cereal grains. The presence of sickle blades and bifacial tools in the flint assemblage suggests cereal harvesting (Rosen, 1982) and woodworking (Barkai, 2005, 2011). Additional information regarding the worked materials and methods requires further research.

Cooking installations have not been found, yet fire use is evident from the presence of micro-charcoal in the site's deposits. The low concentrations of wood ash probably do not reflect properly the intensity of fire use at the site, due to postdepositional dissolution of calcitic ash.

As noted above, the construction of domestic spaces seems to have been based on mud brick or another mud-construction technique.

### *4.3.3. Trade connections*

**(A) Pottery**: A petrographic study of pottery from Dor South (Nickelsberg et al., in press) indicates that the raw materials used for the production of almost the entire ceramic assemblage studied (a total of 25 sherds) were sourced from non-coastal areas. Twenty-two sherds were prepared from a marly paste typical of the Paleocene (66–56 Ma) Taqiye Formation, the closest source of which is more than 10 km away from Dor South, indicating a high probability of imported goods. Two sherds include coastal quartz sand in their paste, indicating coastal production, yet not necessarily at Dor South. These two sherds are poorly preserved (friable) relative to the majority of Taqiye-based sherds (very hard). One sherd was found to include mica and grass temper in its paste, suggesting an Egyptian source. Two such examples have been identified at Ashqelon Barne'a (Cohen-Weinberger, 2022).

**(B) Basalt**: In the Levant basalt was used to prepare a variety of groundstone tools, such as vessels, slab and mortar grinding tools, and weights. Known raw material sources in the southern Levant include primarily inland localities such as the Golan Heights, the Galilee Mountains, and Transjordan basalt flows (Philip and Williams-Thorpe, 2001 Rosenberg and Golani, 2012 and references therein). All basalt items found at Dor South had to be sourced farther away from the site, as basalt outcrops do not occur within a 4–5 km radius from it; the nearest source is Shefeya. Bowls, grinding stones, and spindle whorls made of basalt appear throughout the Levant, from Egypt to Syria, and seem to have been commonly traded objects in EB I. They have often been interpreted as sourced from outcrops in Jordan, the Golan, or the Galilee. For example, Savage (2011) attributes sources based on previously published data on K-Ar dating of basalts. Archaeologists analyzing the EB I layers at Ashqelon suggest a link between copper and basalt trade, with the former being sourced from the Feynan area, the Timna region, or possibly Sinai (Rosenberg and Golani, 2012: 42–43). The traditional trade route proposed for products that would cross the Levant used the extensive networks of wadis and was mainly land based, though maritime trade cannot be ruled out.

This study, based on elemental analysis, shows that most basalt items found at Dor South originate, with a high likelihood, in basalt outcrops in the Carmel and Jezreel Valley regions rather than the eastern Galilee or the Golan. The chemical compositions show that seven of the eight items analyzed here cluster together with basalt reference samples from the Carmel ridge (the Cretaceous Shefeya outcrop) and the Jezreel Valley (the

Miocene Midrach Oz outcrop). The artifact types found at Dor South are relatively simple and do not require a high level of production expertise nor more than a minimal production effort. This observation accords with a general trend reflected also in pottery and copper items becoming less elaborate in comparison with the Chalcolithic period (Milevski, 2013b). We suggest that obtaining basalt from relatively close production centers may also be associated with effort reduction. The closest possible EB I production center, where there was habitation next to Miocene basalt outcrops, was at Megiddo. Basalt items at this site include bowls and tournettes and slabs that were incorporated into the EB I temple (Braun, 1990: 94; Roux and de Miroschedji, 2009: table 1; Adams et al., 2014: 34). Finds from this temple indicate significant basalt quarrying and production capabilities at Megiddo (Adams et al., 2014: 36). Another EB IA settlement in the central coastal plain is ʻEn Esur, where various basalt groundstone tools have been found (Rowan, 2006). As this was a relatively small village during EB IA, located several kilometers from Cretaceous or Miocene basalt outcrops, it is unlikely to have been a production center.

Some weak geochemical clustering may also exist with a few samples from the Golan Heights (Mas'ada and Ein Zivan), which opens up the possibility of more localized networks of basalt quarrying and artisan craftsmanship. Yet, there are no potential production centers in the Golan Heights during this period, as there are no EB I settlements in this region. As Plio-Pleistocene (ca. 5 Ma–12 Ka) basalts also occur in the eastern Galilee, potential production centers include Tel Beth Yerah, Tel Dan, Tel Te'o, Gadot, and Tell esh-Shuna (Braun, 1990: fig. 1; Milevski 2005: map 10; Roux and de Miroschedji, 2009: fig. 1; de Miroschedji, 2013: 309–310; Greenberg 2019: 27–28).

The chemically unique item DS-22 must have originated in a source that was not sampled in this work, and it also matches with no basalt outcrops published by others (Weinstein 2000, 2012; Gluhak and Rosenberg, 2013; Rosenberg et al., 2015), with its high content of Cr, Ni, and Mo concentrations. Interestingly, item DS-26 is also distinguished by a high Mo concentration. The elevated Cr and Ni concentrations found in item DS-22 are exceptional also by comparison with published geochemical data in previous studies (e.g., Weinstein, 2000; Gluhak and Rosenberg, 2013; Gluhak et al., 2022). This suggests a basanite composition unknown in the area. As item DS-22 is also distinguished from all others in its major element composition, it may have been imported to the site from a more distant origin. We propose that it may originate in a mafic ophiolitic rock, with known outcrops in the eastern Mediterranean along the southern Turkish–northern Syrian coast, as well as in Cyprus. As examples of electrum sourced in southern Turkey–northern Syria have been found at Chalcolithic sites in Israel, we propose that the exceptional basalt object DS-22 may have arrived at the site of Dor South either by overland trade with this region or, possibly, via maritime trade with Cyprus.

**(C) Flint**: Preliminary observations on the flint raw materials at Dor South indicate diverse flint sources. As flint-bearing outcrops do not occur on the Carmel coastal plain, the nearest sources for flint nodules suitable for knapping were either in stream beds draining Mount Carmel that transect the coastal plain or directly from outcrops on Mount Carmel; however, more distant sources for flint are possible as well. The presence of Canaanean blades, on the one hand, and the lack of Canaanean blade cores and their production waste, on the other hand, are clear indicators that Canaanean blades were not produced on-site. This observation suggests that these items were obtained through trade with flint knappers from nearby or distant sites, which is supported by previous research concluding that Canaanean blades were manufactured in dedicated workshops, at a limited number of sites and by specialist flint knappers (Milevski, 2013a).

## 5. Conclusions

While Dor South does not represent a complete site, as only the edge of the original settlement is preserved, the micro-archaeological approach of this research enabled an assessment of the site, indicating many similarities with EB IA coastal sites in the south. First, it is similar to sites along the southern coast of Israel in size and layout, being a long strip of ca. 1 km, stretching along the coast (Nickelsberg et al., 2024). Similarities between Dor South and both inland and coastal sites also appear in construction, which is based primarily on mud, and in pottery typologies, as well as flint objects, reflecting a general trend of standardization. Groundstone tools are also similar, representing trade networks utilizing pack animals, which are attested at southern sites (Milevski, 2009; Greenberg, 2019). The flint sickle blades, basalt groundstones, animal bones, and phytolith assemblages show a village economy, primarily autarkic, like other coastal Neolithic, Chalcolithic, and EB IA sites (e.g., Gophna, 1997; Garfinkel and Dag, 2008).

The scarcity of marine mollusks other than *Glycymeris* sp. and absence of fish bones suggest that the site inhabitants did not rely on marine resources; however, this may be a result of poor preservation of fish remains and/or the small sample size of the excavated area relative to the extent of this large settlement. The dominance of nonlocal pottery at this site, as shown petrographically by Nickelsberg et al. (in press), may indicate a seasonal rather than permanent site. This being said, given the magnitude of this settlement, it is unlikely to have been ephemeral. If the pottery assemblage from the excavated area indeed represents the entire site, we may argue that Dor South was a coastal settlement not adapted to coastal life, that relied on inland resources also for its pottery, as opposed to other contemporary coastal settlements. Other resources procured inland include basalt, using networks reaching the Jezreel Valley (a one-day walk to the Miocene Midrach Oz outcrops), and possibly even networks of a few days' walk to the eastern Galilee and the Golan. The utilization of networks of basalt during EB I was discussed also for the coastal Ashqelon sites, suggesting sources as far as Transjordan. Though flint was probably procured from nearby sources on Mount Carmel, the Canaanean blades were most probably produced in an expert workshop farther away from the site and also obtained through trade networks. A further geochemical study of the flint sources may shed more light on the origins of the Canaanean blades and other items unearthed at the site.

Overall, the evidence retrieved by the small-scale excavation on the edge of the EB IA site of Dor South suggests this was a large permanent settlement that engaged in subsistence agropastoralism, as well as in trade with inland settlements. Future excavations may reveal evidence of the use of marine resources, macrobotanical remains, structures and/or maritime trade connections, as in other large EB IA coastal sites.

## Acknowledgements

This research was supported by the Israel Science Foundation: Grant No. 697/20 to R.S-G. We would like to thank Karem Sa'id, Haifa District Archaeologist, and Limor Talmi of the IAA for their support during the excavations.

## References

Adams, M.J., David, J., Homsher, R.S., Cohen, M.E., 2014. The rise of a complex society: new evidence from Tel Megiddo East in the late fourth millennium. *Near Eastern Archaeology* 77 (1), 32–43.

Albert, R.M., Shahack-Gross, R., Cabanes, D., Gilboa, A., Lev-Yadun, S., Portillo, M., Sharon, I., Boaretto, E., Weiner, S., 2008. Phytolith-rich layers from the Late Bronze and Iron Ages at Tel Dor (Israel): mode of formation and archaeological significance. *Journal of Archaeological Science* 35 (1), 57–75. https://doi.org/10.1016/j.jas.2007.02.015.

Arnold, E.R., Hartman, G., Greenfield, H.J., Shai, I., Babcock, L., Maeir, A.M., 2016. Isotopic evidence for early trade in animals between Old Kingdom Egypt and Canaan. *PLoS One* 11 (1–12), e0157650. https://doi.org/10.1371/journal.pone.0157650.

Balasse, M., Smith, A.B., Ambrose, S.H., Liegh, S.R., 2003. Determining sheep birth seasonality by analysis of tooth enamel oxygen isotope ratios: the Late Stone Age site of Kasteelberg (South Africa). *Journal of Archaeological Science* 30 (2), 205–215.

Banning, E.B., 2019. It's a small world: work, family life and community in the Late Neolithic, in: Yasur-Landau, A., Cline, E.H., Rowan Y.M. (Eds.), *The Social Archaeology of the Levant from Prehistory to the Present*. Cambridge University Press, Cambridge and New York, pp. 98–121.

Bar, S., Zutovski, K., Hruby, K., Ujma, C., 2021. Excavations at the Early Bronze Age I site Fazael 4: the 2017–2020 seasons. *Journal of the Israel Prehistoric Society* 51, 261–303.

Barkai, R., 2005. *Flint and Stone Axes as Cultural Markers: Socio-economic Changes as Reflected in Holocene Flint Tool Industries of the Southern Levant*. Ex Oriente, Berlin.

Barkai, R., 2011. The evolution of Neolithic and Chalcolithic woodworking tools and the intensification of human production: axes, adzes, and chisels from the southern Levant, in: Davis, V., Edmonds, M. (Eds.), *Stone Axe Studies III*. Oxbow, Oxford, pp. 39–54.

Bar-Matthews, M., Ayalon, A., 2011. Mid-Holocene climate variations revealed by high-resolution speleothem records from Soreq Cave, Israel and their correlation with cultural changes. *The Holocene* 21 (1), 163–171. https://doi.org/10.1177/0959683610384165.

Berna, F., Behar, A., Shahack-Gross, R., Berg, J., Boaretto, E., Gilboa, A., Sharon, I., Shalev, S., Shilstein, S., Yahalom-Mack, N., Zorn, J.R., Weiner, S., 2007. Sediments exposed to high temperatures: reconstructing pyrotechnological processes in Late Bronze and Iron Age strata at Tel Dor (Israel). *Journal of Archaeological Science* 34, 358–373.

Braun, E., 1990. Basalt bowls of the EB I horizon in the southern Levant. *Paléorient* 16 (1), 87–96.

Braun, E., 1992. Palmaḥim Quarry 1989/1990. *Excavations and Surveys in Israel* 10, 21–23.

Braun, E., 2014. Observations on contacts between the Nile Valley and the southern Levant in late prehistory prior to Dynasty 0, in: Jucha, M.A., Dębowska-Ludwin, J., Kolodziejczyk, P. (Eds.), *Aegyptus est imago caeli: Studies Presented to Krzysztof M. Cialowicz on His 60th Birthday*. Institute of Archaeology, Jagiellonian University, Krakow, pp. 223–234.

Broodbank, C., 2013. *The Making of the Middle Sea: A History of the Mediterranean from the Beginning to the Emergence of the Classical World*. Oxford University Press, Oxford.

Chesson, M. S., 2019. The southern Levant during the Early Bronze Age I–III, in: Yasur-Landau, A., Cline, E. H., Rowan, Y. M. *The Social Archaeology of the Levant from Prehistory to the Present*. Cambridge University Press, Cambridge, pp. 163–182.

Cohen-Weinberger, A., 2022. Petrographic analysis of selected vessels, in: Golani A. (Ed.), *Ashqelon Barne'a: The Early Bronze Age Site,* II: *The Finds* (IAA Reports 70). Israel Antiquities Authority, Jerusalem, pp. 91– 99.

Cropper, J., 1902. The geographical distribution of Anopheles and malarial fever in upper Palestine. *Journal of Hygiene* 2, 47–57.

Danin, A., Fragman-Sapir, O., 2009. *Vegetation of Israel and Neighboring Countries*. https://flora.org.il/en/books/vegetation-of-israel-and-neighboring-countries/ (accessed 28 February 2024).

Galili, E., Zvieli, D., Weinstein-Evron, M., 2005. Holocene sea level changes and landscape evolution on the northern Carmel Coast, Israel. *Méditerranée* 1 (2), 79–86.

Garfinkel, Y., 2014. The Levant in the Pottery Neolithic and Chalcolithic periods, in: Renfrew C., Bahn P. (Eds.), *The Cambridge World Prehistory*. Cambridge University Press, New York, pp. 1439–1461.

Garfinkel, Y., Dag, D., 2008. *Neolithic Ashqelon* (Qedem 47). Institute of Archaeology, Hebrew University, Jerusalem.

Gluhak, T.M., Rosenberg, D., 2013. Geochemical discrimination of basaltic sources as a tool for provenance analyses of bifacial tools in the southern Levant: first results from the Jezreel Valley, Israel. *Journal of Archaeological Science* 40, 1611–1622.

Gluhak, T.M., Ebeling, J., Rosenberg, D., 2022. Geochemical provenance studies of basalt vessel preforms from the Iron Age workshop at Tel Hazor, Israel, and potential geological sources. *Archaeometry* 64 (1), 25–38.

Golani, A., 2008. The Early Bronze Age site of Ashkelon, Afridar—Area M. *'Atiqot* 60, 19–51.

Golani, A., 2013. The transition from the Late Chalcolithic to the Early Bronze I in southwestern Canaan: Ashkelon as a case for continuity. *Paléorient* 39 (1), 95–110.

Golani, A., 2019a. Architecture and settlement planning, in: Golani, A. (Ed.), *Ashqelon Barne'a: The Early Bronze Age Site,* I: *The Excavations* (IAA Reports 65). Israel Antiquities Authority, Jerusalem, pp. 249–269.

Golani, A. (Ed.), 2019b. *Ashqelon Barne'a: The Early Bronze Age Site,* I: *The Excavations* (IAA Reports 65). Israel Antiquities Authority, Jerusalem.

Golani, A., 2022. The site in context: summary and conclusions. in: Golani, A. (Ed.), *Ashqelon Barne'a: The Early Bronze Age Site,* II: *The Finds* (IAA Reports 70). Israel Antiquities Authority, Jerusalem, pp. 371–385.

Golani, A., Pasternak, M.D., 2020. Ashqelon Afridar, Area O-2: Early Bronze Age IA remains. *Hadashot Arkheologiyot–Excavations and Surveys in Israel* 132, 1–23. https://www.hadashot-esi.org.il/report_detail_eng.aspx?id=25875&mag_id=128.

Golani, A., Talis, S., 2022. The pottery assemblage, in: Golani, A. (Ed.), *Ashqelon Barne'a: The Early Bronze Age Site,* II: *The Finds* (IAA Reports 70). Israel Antiquities Authority, Jerusalem, pp. 1–89.

Gophna, R., 1997. The southern coastal troughs as EB I subsistence areas. *Israel Exploration Journal* 47, 155–161.

Gophna, R., Liphschitz, N., 1996. The Ashkelon trough settlements in the Early Bronze Age I: new evidence of maritime trade. *Tel Aviv* 23, 143–153.

Goring-Morris, N.A., Belfer-Cohen, A., 2014. The southern Levant (Cisjordan) during the Neolithic period, in: Steiner M.L., Killebrew, A.E. (Eds.), *The Oxford Handbook of the Archaeology of the Levant, c. 8000–332 BCE*. Oxford University Press, Oxford, pp. 147–169.

Greenberg, R., 2019. *The Archaeology of the Bronze Age Levant*. Cambridge University Press, Cambridge.

Gur-Arieh, S., Mintz, E., Boaretto, E., Shahack-Gross, R., 2013. An ethnoarchaeological study of cooking installations in rural Uzbekistan: development of a new method for identification of fuel sources. *Journal of Archaeological Science* 40, 4331–4347.

Higgs, E.S., Vita-Finzi, C., 1972. Prehistoric economies: a territorial approach, in: Higgs E.S. (Ed.), *Papers in Economic Prehistory: Studies by Members and Associates of the British Academy Major Research Project in the Earl*. Cambridge University Press, Cambridge, pp. 27–36.

Inizan, M.L., Reduron-Ballinger, M., Roche, H., Tixier, J., 1999. *Technology and Terminology of Knapped Stone*. Cercle de Recherches et d'Etudes Préhistorique, Nanterre.

International Committee for Phytolith Taxonomy (ICPT), 2019. International Code for Phytolith Nomenclature (ICPN) 2.0. *Annals of Botany* 124 (2), 189–199. https://doi.org/10.1093/aob/mcz064.

Karkanas, P., Goldberg, P., 2018. *Reconstructing Archaeological Sites: Understanding the Geoarchaeological Matrix*. John Wiley & Sons, Hoboken.

Katz, O., Cabanes, D., Weiner, S., Maeir, A.M., Boaretto, E., Shahack-Gross, R., 2010. Rapid phytolith extraction for analysis of phytolith concentrations and assemblages during an excavation: an application at Tell es-Safi/Gath, Israel. *Journal of Archaeological Science* 37, 1557–1563.

Ktalav, I., 2022. The mollusks, in: Golani, A. (Ed.), *Ashqelon Barne'a: The Early Bronze Age Site,* II: *The Finds* (IAA Reports 70). Israel Antiquities Authority, Jerusalem, pp. 347–358.

Langgut, D., Adams, M.J., Finkelstein, I., 2016. Climate, settlement patterns and olive horticulture in the southern Levant during the Early Bronze and Intermediate Bronze Ages (c. 3600–1950 BC). *Levant* 48 (2), 117–134.

Le Maitre, R.W., 1989. *A Classification of Igneous Rocks and Glossary of Terms*. Blackwell, Oxford.

Madella, M., Alexandre, A., Ball, T., 2005. International Code for Phytolith Nomenclature 1.0. *Annals of Botany* 96 (2), 253–260. https://doi.org/10.1093/aob/mci172.

Milevski, I., 2005. *Local Exchange in Early Bronze Age Canaan*. Unpublished Ph.D. dissertation, Tel Aviv University.

Milevski, I., 2009. Local exchange in the southern Levant during the Early Bronze Age: a political economy viewpoint. *Antiquo Oriente* 7, 125–159.

Milevski, I., 2013a. The exchange of flint tools in the southern Levant during the Early Bronze Age. *Lithic Technology* 38 (3), 202–219.

Milevski, I., 2013b. The transition from the Chalcolithic to the Early Bronze Age of the southern Levant in socio-economic context. *Paléorient* 39 (1), 193–208.

Milevski, I., Liran, R., Getzov, N., 2014. The Early Bronze Age town of Ein Zippori in the Galilee (Israel). *Antiquity* 88 (339), 2–5.

Miroschedji, P. de, 2013. The southern Levant (Cisjordan) during the Early Bronze Age, in: Steiner M.L., Killebrew A.E. (Eds.), *The Oxford Handbook of the Archaeology of the Levant, c. 8000– 332 BCE*. Oxford University Press, Oxford, pp. 307–329.

Nickelsberg, R., Arkin-Shalev, E., Yasur-Landau, A., 2022. Dor (South) underwater survey. *Hadashot Arkheologiyot–Excavations and Surveys in Israel* 134. https://hadashot-esi.org.il/report_detail_eng.aspx?id=26230&mag_id=134.

Nickelsberg, R., Shahack-Gross, R., 2021. Dor South. *Hadashot Arkheologiyot–Excavations and Surveys in Israel* 133. https://www.hadashot-esi.org.il/report_detail_eng.aspx?id=26051&mag_id=133.

Nickelsberg, R., Shahack-Gross, R., Yasur-Landau, A., 2024. The Early Bronze Age I coastal settlements of Israel: a new phenomenon or a long-lived settlement tradition? in: Yasur-Landau, A., Gambash, G., Levy, T.E. (Eds.), *Mediterranean Resilience: Collapse and Adaptation in Antique Maritime Societies*. Equinox, Sheffield, pp. 66–91.

Nickelsberg, R., Shapiro, A., Cohen-Weinberger, A., Paz, Y., Elad, I., Yasur-Landau, A., Shahack-Gross, R., In press. Economic strategies of the EB IA identified through ceramic petrography of the coastal site of Dor South and the inland site of ʻEn Esur: consequences leading up to urbanism in the southern Levant. *ʻAtiqot*.

Ogloblin Ramirez, I., Galili, E., Be'eri, R., Golan, D., Krakovsky, M., Dayan, A., Shalem, D., Shahack-Gross, R., 2020. Heated mud bricks in submerged and coastal southern Levant Pre-Pottery Neolithic C and Late Pottery Neolithic/Early Chalcolithic settlements: diachronic changes in technology and their social implications. *Journal of Archaeological Science Report* 30, 102220. https://doi.org/10.1016/j.jasrep.2020.102220.

Olami, Y., Sender, S., Oren, E., 2005. *Archaeological Survey of Israel, Map of Dor (30)*. Israel Antiquities Authority, Jerusalem.

Paz, Y., 2002. Fortified settlements of the EB IB and the emergence of the first urban system. *Tel Aviv* 29 (2), 238–261.

Perlès, C., 1987. *Les industries lithiques taillées de Franchthi Argolide (Grèce),* I: *Présentation générale et industries Paléolithiques*. Indiana University Press, Terre Haute.

Philip, G., Williams-Thorpe, O., 2001. The production and consumption of basalt artefacts in the southern Levant during the 5th–4th millennia BC: a geochemical and petrographic investigation, in: *Archaeological Sciences '97: Proceedings of the Conference Held at the University of Durham, 2nd–4th September 1997* (BAR International Series 939). Archaeopress, Oxford, pp. 11–30.

Porat, N., Wintle, A.G., Ritte, M., 2004. Mode and timing of kurkar and hamra formation, central coastal plain, Israel. *Israel Journal of Earth Sciences* 53 (1), 13–25.

Rosen, A.M., 2007. *Civilizing Climate: Social Responses to Climate Change in the Ancient Near East*. Altamira Press, Lanham, MD.

Rosen, S.A., 1982. Flint sickle-blades of the late protohistoric and early historic periods in Israel. *Tel Aviv* 9 (2), 139–145.

Rosen, S., 1997. *Lithic after the Stone Age: A Handbook of Stone Tools from the Levant*. AltaMira Press, Walnut Creek.

Rosenberg, D., Golani, A., 2012. Ground stone tools of a 'coppersmiths' community: understanding stone-related aspects of the Early Bronze Age site of Ashqelon Barnea. *Journal of Mediterranean Archaeology* 25 (1), 27–51.

Rosenberg, D., Shimelmitz, R., Gluhak, T.M., Assaf, A., 2015. The geochemistry of basalt handaxes from the Lower Palaeolithic site of Ma' ayan Baruch, Israel: a perspective on raw material selection. *Archaeometry* 57, 1–19.

Roux, V., Miroschedji, P. de, 2009. Revisiting the history of the potter's wheel in the southern Levant. *Levant* 41 (2), 155–173.

Rowan, Y.M., 2006. The groundstone assemblages, in: Yannai, E. (Ed.), *'En Esur ('Ein Asawir),* I: *Excavations at a Protohistoric Site in the Coastal Plain of Israel* (IAA Reports 31). Israel Antiquities Authority, Jerusalem, pp. 211–250.

Savage, S.H., 2011. From Maadi to the plain of Antioch: what can basalt spindle whorls tell us about overland trade in the Early Bronze I Levant? in: Chesson, M.S. (Ed.), *Daily Life, Materiality, and Complexity in Early Urban Communities of the Southern Levant: Papers in Honor of Walter E. Rast and R. Thomas Schaub*. Eisenbrauns, Winona Lake, pp. 119–138.

Segev, A., Sass, E., 2009. *The Geological Map of Israel, 1:50,000, Sheet 3-III: Atlit*. Israel Geological Survey, Jerusalem.

Sellet, F., 1993. Chaîn opératoire: the concept and its applications. *Lithic Technology* 18 (1/2), 106–112.

Sharvit, J., Galili, E., Rosen, B., Brink, E.C.M. van den, 2002. Predynastic maritime traffic along the Carmel Coast of Israel: a submerged find from north Atlit Bay, in: Brink, E.C.M. van den, Yannai, E. (Eds.), *In Quest of Ancient Settlement and Landscapes: Archaeological Studies in Honour of Ram Gophna*. Ramot Publishing, Tel Aviv University, Tel Aviv, pp. 159–166.

Stoops, G., 2003. *Guidelines for Analysis and Description of Soil and Regolith Thin Sections*. Soil Science Society of America, Madison.

Tixier, J., 1963. *Typologie du l'épipaléolithique de Maghreb*. Arts et métiers graphiques, Paris.

Tuross, N., Behrensmeyer, A.K., Eanes, E.D., Fisher, L.W., Hare, P.E., 1989. Molecular preservation and crystallographic alterations in a weathering sequence of wildebeest bones. *Applied Geochemistry* 4 (3), 261–270.

Weinstein, Y., 2000. Spatial and temporal geochemical variability in basin-related volcanism, northern Israel. *Journal of African Earth Sciences* 30 (4), 865–886.

Weinstein, Y., 2012. Transform faults as lithospheric boundaries, an example from the Dead Sea Transform. *Journal of Geodynamics* 54, 21–28.

Wengrow, D., 2006. *The Archaeology of Early Egypt: Social Transformations in North-East Africa, c. 10,000 to 2,650 BC*. Cambridge University Press, Cambridge.

Yannai, E., 2006. *'En Esur ('Ein Asawir),* I: *Excavations at a Protohistoric Site in the Coastal Plain of Israel* (IAA Reports 31). Israel Antiquities Authority, Jerusalem.

Yannai, E., Braun, E., 2001. Anatolian and Egyptian imports from late EB I at Ain Assawir, Israel. *Bulletin of the American Schools of Oriental Research* 321, 41–56.

Zidane, A., Bar-Oz, G., 2022. The faunal remains, in: Golani, A. (Ed.), *Ashqelon Barne'a: The Early Bronze Age Site,* II: *The Finds* (IAA Reports No. 70). Israel Antiquities Authority, Jerusalem, pp. 218–328.

# Appendix A: Detailed materials, methods, and results for basalt geochemistry study

Ilaria Patania, Department of Maritime Civilizations, University of Haifa (ilariapat@gmail.com), and Nadya Teutsch, Geological Survey of Israel, Jerusalem (nadya.teutsch@gsi.gov.il)

All geological (n = 11) and archaeological (n = 8) basalt samples (Tables A.1, A.2, Fig. A.1) were sonicated in deionized water at 5–20-minute increments to dislodge adhering sediment, which was then transferred to 50 ml polypropylene tubes and centrifuged at 4000 rpm for 10 minutes. The solution was poured out, and the sediment, as well as the cleaned basalt item, was placed overnight in a drying oven set to 30°C. The dry sediment was stored for future paleobotanical analyses.

The cleaned archaeological items were examined macroscopically using a hand lens, described, and photographed; 3D images were then created with an HP 3D Structured Light Scanner Pro S3 equipped with an automatic turntable. The geological samples were examined with a hand lens and described. Following documentation, a chip of about 5 gr was cut close to the core of each sample (to reduce chances of contamination), using a non-cooled commercial rock saw, and the edges chipped away with pincers to remove weathering crusts.

The chip was prepared for elemental analysis to quantify the concentrations of major (e.g., oxides), minor, and trace elements in all samples. The sample was sonicated in a 1M HCl solution for 10 minutes, soaked in a 1M HCl solution for 45 minutes, and then sonicated in deionized water for 5 minutes. When this treatment did not remove all visible crusts, the sample was further sonicated in a 1M HCl solution at 5-minute increments until visible crusts were removed. These were then washed in deionized water. All samples were dried overnight in an oven set to 50°C. The clean and dry samples were pulverized for further dissolution for elemental analyses. Major and minor element concentrations (Si, Al, Fe, Ti, Mn, Ca, Mg, Na, K, P, Sr, and Ba and the trace element Zr) were determined by inductively coupled plasma optical emission spectrometry (ICP-OES), using a PerkinElmer Optima 5300 ICP-OES, following a lithium metaborate fusion in platinum crucibles (Brenner et al., 1980). Additional minor elements and trace metals (Be, V, Cr, Co, Ni, Cu, Zn, Rb, Y, Zr, Nb, Mo, Hf, Ta, Pb, Th, and U) concentrations were determined by inductively coupled plasma mass spectrometry (ICP-MS), using a PerkinElmer NexION 330D ICP-MS, following dissolution by sodium peroxide sintering in zirconium crucibles (Brenner et al., 1980; Yu et al., 2001). Rare earth elements (REE; La to Lu) were processed and analyzed similarly to the trace elements. Three certified reference materials (CRMs) of basalts (JB-1, JB-3, and NBS-688) were processed and analysed along with the samples for quality control. Accuracy, precision, and procedural reproducibility per element are presented in Table A.3.

Elemental concentrations results were plotted in a correlation matrix, and pairs of elements with high correlations within and between the geological and archaeological samples were further examined.

**Table A.1.** List of archaeological samples analyzed, their typology, macroscopic description, and archaeological context

| Item no. | Typology | Macro-description | Stratigraphic context |
|---|---|---|---|
| 2 | Thin-walled vessel (body) | Microcrystalline; vesicles > 2 mm | Topsoil (Layer 5) |
| 20a | Possible pedestal of raised bowl | Microcrystalline; no visible vesicles | Topsoil (Layer 5) |
| 22 | Two-handed(?) upper grinding stone | Microcrystalline; pyroclastic, with ~5 mm wide round vesicles. Some vesicles are coated internally by calcitic amigdaloids. | Fine-grained gray deposit (Layer 4) |
| 23 | Spindle whorl | Porphyric texture, with mm size olivine and iddingsite crystals; no visible vesicles | Surface find |
| 24 | Intact upper grinding stone | Microcrystalline; pyroclastic, with bimodal porosity of ~1 and ~5 mm wide vesicles. Some vesicles are filled or coated internally by calcitic amigdaloids | Surface find |
| 25 | Rim of open, flaring-walled bowl | Microcrystalline; vesicles > 2 mm | Surface find |
| 26 | Small one-handed upper grinding stone | Microcrystalline; pyroclastic, with bimodal porosity of ~1 and ~5 mm wide vesicles | Fine-grained gray deposit (Layer 4) |
| 27 | Vessel base | Microcrystalline; no visible vesicles | Mechanical trench; 64 cm below surface (Layer 5 or 4) |

**Table A.2.** List of geological samples analyzed, their location in Israel, geological context, and macroscopic description

| Sample no. | Locality | Geological information | Macro-description |
|---|---|---|---|
| GK-5 | Menashe Hills, Giv'at Kipod 32°36′33.2″N 35°07′26.1″E | Miocene; Lower Basalt | Microcrystalline; low to no visible vesicles |
| MO-7 | Jezreel Valley, Midrach Oz 32°36′41.6″N 35°08′11.6″E | Miocene; Lower Basalt | Microcrystalline with visible iddingsite and a few calcitic concretions (no clearly visible amigdaloids); vesicles between 1 and 5 mm |
| S-8 | Carmel ridge, Ofer 32°37′36.7″N 34°58′42.1″E | Cretaceous; Shefeya Basalt | Microcrystalline with iddingsite and calcitic amigdaloids; vesicles between 1 and 3 mm |
| M-10 | Golan Heights, Mas'ada 33°13′45.1″N 35°44′55.4″E | Late Pleistocene; Sa'ar lava flow | Microcrystalline with thin red staining bands; no visible vesicles |
| MG-12 | Golan Heights, Merom Golan 33°08′49.9″N 35°46′56.7″E | Late Pleistocene; Golan lava flow | Microcrystalline with > 5 mm vesicles |
| MG-13 | Golan Heights, Merom Golan 33°08′21.7″N 35°46′11.7″E | Early Pleistocene; Muweisse lava flow | Microcrystalline; no visible vesicles |
| EZ-14 | Golan Heights, Ein Zivan 33°05′27.2″N 35°47′25.7″E | Middle/Late Pleistocene; Ein Zivan lava flow | Microcrystalline; elongated and oriented vesicles between 3 and 10 mm |

**Table A.3.** Accuracy, precision, and procedural reproducibility per element (majors appearing as oxides)

| | Accuracy | Precision | Reproducibility |
|---|---|---|---|
| $SiO_2$ | 3 | 0.1 | 1.3 |
| $Al2O_3$ | 4 | 1.0 | 2.0 |
| $Fe_2O_3$ | 3 | 0.2 | 5.0 |
| $TiO_2$ | 5 | 0.5 | 2.0 |
| MnO | 3 | 0.8 | 2.0 |
| CaO | 1 | 0.8 | 1.1 |
| MgO | 2 | 1.2 | 2.0 |
| $Na_2O$ | 1 | 0.4 | 2.0 |
| $K_2O$ | 6 | 1.5 | 1.5 |
| $P_2O_5$ | 20 | 10.0 | 20.0 |
| Be | 6 | 1.2 | 0.3 |
| V | 4 | 2.0 | 1.5 |
| Cr | 3 | 0.8 | 4.0 |
| Co | 3 | 1.4 | 6.0 |
| Ni | 4 | 1.0 | 3.0 |
| Cu | 5 | 1.5 | 1.3 |
| Zn | 5 | 1.0 | 3.0 |
| Rb | 1 | 0.2 | 1.4 |
| Sr | 1 | 0.7 | 2.0 |
| Y | 7 | 4.0 | 5.0 |
| Zr | 7 | 1.0 | 1.3 |
| Nb | 8 | 1.3 | 3.0 |
| Mo | 4 | 1.0 | 0.4 |
| Ba | 5 | 0.7 | 2.0 |
| La | 4 | 3.0 | 5.0 |
| Ce | 4 | 3.0 | 3.0 |
| Pr | 5 | 1.5 | 4.0 |
| Nd | 5 | 2.0 | 1.1 |
| Sm | 7 | 0.8 | 2.0 |
| Eu | 2 | 1.4 | 0.9 |
| Gd | 4 | 2.0 | 1.5 |
| Tb | 5 | 4.0 | 2.0 |
| Dy | 1 | 3.0 | 1.4 |
| Ho | 1 | 1.0 | 0.2 |
| Er | 1 | 0.3 | 0.3 |
| Tm | 3 | 1.1 | 2.0 |
| Yb | 7 | 1.4 | 3.0 |
| Lu | 5 | 2.0 | 3.0 |
| Hf | 1 | 3.0 | ND |
| Ta | 4 | 3.0 | 2.0 |
| Pb | 4 | 1.3 | 1.0 |
| Th | 8 | 4.0 | 4.0 |
| U | 3 | 3.0 | 0.9 |

[1] Accuracy (± %) maximal value for each element based on analysis of three CRMs of basalts (JB-1, JB-3, NBS-688) dissolved and analyzed alongside the samples. For majors, each standard was processed twice, and for traces and REE, each standard was processed once.

[2] Precision presented as RSD (%) for each element based on triplicate analyses of the CRM JB-1 (at the beginning, middle, and end of analytical session).

[3] Reproducibility presented as RSD (%) for majors based on four separate processing of JB-1 (dissolution and analyses) and as % difference for traces and REE based on two separate processing of JB-1.

**Table 4.** Major (e.g., oxides) and trace elements of geological (highlighted in gray) and archaeological samples

| W% | MO-7 | M-10 | MG-12 | GK-5 | S-8 | G-13 | EZ-14 | DS-25 | DS-20A | DS-22 | DS-23 | DS-24 | DS-26 | DS-27 | DS-2 |
|---|---|---|---|---|---|---|---|---|---|---|---|---|---|---|---|
| $SiO_2$ | 47.50 | 45.66 | 44.53 | 44.67 | 46.59 | 44.36 | 45.27 | 46.74 | 47.54 | 43.45 | 48.46 | 45.92 | 47.39 | 47.29 | 47.05 |
| **$TiO_2$** | 2.48 | 2.71 | 2.70 | 3.12 | 2.97 | 3.00 | 3.05 | 2.15 | 1.78 | 2.49 | 2.30 | 2.41 | 2.65 | 2.42 | 2.09 |
| $Al_2O_3$ | 16.48 | 16.57 | 13.50 | 13.91 | 14.44 | 14.35 | 14.10 | 15.24 | 15.23 | 13.49 | 16.22 | 15.26 | 14.63 | 16.03 | 15.25 |
| **$Fe_2O_3$** | 14.81 | 12.06 | 11.68 | 12.71 | 14.96 | 12.51 | 14.02 | 12.45 | 12.66 | 14.45 | 13.74 | 12.67 | 12.40 | 12.47 | 13.06 |
| **MnO** | 0.32 | 0.18 | 0.16 | 0.17 | 0.10 | 0.17 | 0.16 | 0.17 | 0.18 | 0.18 | 0.13 | 0.18 | 0.16 | 0.17 | 0.17 |
| **MgO** | 2.82 | 4.92 | 8.61 | 7.69 | 4.85 | 8.84 | 8.13 | 5.95 | 7.11 | 7.97 | 3.70 | 5.34 | 5.85 | 4.94 | 6.64 |
| **CaO** | 8.12 | 9.68 | 10.19 | 9.62 | 7.03 | 8.68 | 9.00 | 10.85 | 9.97 | 10.19 | 7.56 | 11.21 | 9.87 | 10.30 | 10.36 |
| $Na_2O$ | 3.36 | 4.43 | 3.91 | 3.92 | 2.62 | 3.15 | 2.85 | 3.34 | 3.43 | 5.22 | 3.37 | 3.32 | 3.24 | 3.49 | 3.06 |
| **$K_2O$** | 0.62 | 1.62 | 1.50 | 1.93 | 1.66 | 1.27 | 1.20 | 0.75 | 0.60 | 0.96 | 0.58 | 1.06 | 1.24 | 0.90 | 0.66 |
| **$P_2O_5$** | 0.28 | 1.35 | 1.78 | 1.13 | 0.80 | 1.49 | 0.84 | 0.23 | 0.18 | 0.68 | 0.28 | 0.89 | 0.68 | 0.53 | 0.42 |
| **LOI** | 2.94 | -0.14 | 0.55 | 0.45 | 3.85 | 1.38 | 1.23 | 1.33 | 0.37 | 0.76 | 3.45 | 0.97 | 1.28 | 0.87 | 0.75 |
| **mg/kg** | | | | | | | | | | | | | | | |
| **Be** | 0.7 | 1.7 | 1.6 | 1.9 | 1.9 | 1.5 | 1.4 | 0.9 | 0.8 | 0.7 | 0.6 | 1.4 | 1.2 | 1.1 | 0.9 |
| **V** | 255.0 | 230.0 | 175.0 | 180.0 | 175.0 | 165.0 | 175.0 | 215.0 | 200.0 | 190.0 | 230.0 | 235.0 | 220.0 | 220.0 | 195.0 |
| **Cr** | 360.0 | 90.0 | 430.0 | 170.0 | 495.0 | 480.0 | 455.0 | 575.0 | 465.0 | 720.0 | 355.0 | 175.0 | 420.0 | 215.0 | 475.0 |
| **Co** | 63.0 | 38.0 | 46.0 | 42.0 | 48.0 | 51.0 | 50.0 | 43.0 | 50.0 | 61.0 | 54.0 | 41.0 | 45.0 | 39.0 | 44.0 |
| **Ni** | 243.0 | 64.0 | 285.0 | 114.0 | 323.0 | 320.0 | 325.0 | 242.0 | 236.0 | 519.0 | 224.0 | 90.0 | 267.0 | 109.0 | 247.0 |
| **Cu** | 60.0 | 50.0 | 47.0 | 61.0 | 68.0 | 53.0 | 64.0 | 58.0 | 58.0 | 63.0 | 62.0 | 73.0 | 44.0 | 39.0 | 55.0 |
| **Zn** | 120.0 | 120.0 | 120.0 | 120.0 | 150.0 | 120.0 | 130.0 | 100.0 | 97.0 | 110.0 | 145.0 | 110.0 | 115.0 | 110.0 | 100.0 |
| **Rb** | 3.5 | 11.0 | 13.0 | 13.0 | 9.5 | 5.8 | 4.5 | 3.5 | 2.4 | 5.0 | 4.2 | 6.2 | 8.0 | 5.4 | 3.0 |
| **Sr** | 490.0 | 1200.0 | 1590.0 | 305.0 | 775.0 | 440.0 | 730.0 | 800.0 | 525.0 | 500.0 | 1150.0 | 745.0 | 1315.0 | 985.0 | 385.0 |
| **Y** | 20.0 | 35.0 | 25.0 | 34.0 | 31.0 | 23.0 | 32.0 | 22.0 | 22.0 | 21.0 | 17.0 | 32.0 | 22.0 | 25.0 | 30.0 |
| **Zr** | 115.0 | 255.0 | 270.0 | 110.0 | 130.0 | 105.0 | 195.0 | 185.0 | 170.0 | 155.0 | 245.0 | 230.0 | 250.0 | 200.0 | 135.0 |
| **Nb** | 9.0 | 41.0 | 41.0 | 62.0 | 36.0 | 47.0 | 43.0 | 11.0 | 9.0 | 16.0 | 10.0 | 21.0 | 20.0 | 21.0 | 18.0 |
| **Mo** | 3.6 | 5.1 | 6.9 | 4.2 | 8.5 | 6.9 | 7.7 | 7.9 | 4.1 | 28.0 | 9.5 | 6.1 | 24.0 | 4.4 | 6.6 |
| **Ba** | 385.0 | 615.0 | 890.0 | 160.0 | 360.0 | 165.0 | 970.0 | 605.0 | 230.0 | 200.0 | 545.0 | 355.0 | 820.0 | 505.0 | 170.0 |
| **La** | 14.0 | 64.0 | 79.0 | 68.0 | 39.0 | 61.0 | 52.0 | 13.0 | 11.0 | 24.0 | 13.0 | 38.0 | 31.0 | 23.0 | 23.0 |
| **Ce** | 29.0 | 119.0 | 144.0 | 129.0 | 75.0 | 115.0 | 103.0 | 29.0 | 23.0 | 51.0 | 26.0 | 82.0 | 61.0 | 50.0 | 51.0 |
| **Pr** | 4.0 | 14.0 | 17.0 | 15.0 | 9.1 | 14.0 | 13.0 | 3.8 | 3.1 | 6.1 | 3.5 | 10.0 | 7.3 | 6.5 | 6.2 |
| **Nd** | 18.0 | 54.0 | 64.0 | 56.0 | 36 | 52.0 | 51.0 | 17.0 | 14.0 | 26.0 | 16.0 | 42.0 | 31.0 | 28.0 | 26.0 |
| **Sm** | 4.5 | 10.0 | 11.0 | 11.0 | 7.7 | 9.5 | 9.8 | 4.3 | 3.5 | 5.6 | 3.7 | 8.4 | 6.3 | 6.1 | 5.7 |
| **Eu** | 1.8 | 3.2 | 3.6 | 3.4 | 2.6 | 3.1 | 3.3 | 1.6 | 1.4 | 2.0 | 1.5 | 2.8 | 2.3 | 2.2 | 2.0 |
| **Gd** | 4.8 | 9.2 | 9.9 | 9.6 | 7.0 | 8.5 | 8.7 | 4.7 | 3.8 | 5.4 | 3.9 | 8.2 | 6.2 | 6.0 | 5.7 |
| **Tb** | 0.8 | 1.3 | 1.3 | 1.3 | 1.0 | 1.1 | 1.2 | 0.8 | 0.7 | 0.8 | 0.6 | 1.2 | 0.9 | 0.9 | 0.9 |
| **Dy** | 4.1 | 5.8 | 5.0 | 5.7 | 4.4 | 4.6 | 5.3 | 4.0 | 3.4 | 3.6 | 3.2 | 5.6 | 4.3 | 4.5 | 4.2 |
| **Ho** | 0.7 | 1.0 | 0.8 | 1.0 | 0.7 | 0.7 | 0.9 | 0.7 | 0.7 | 0.6 | 0.6 | 0.9 | 0.7 | 0.8 | 0.8 |
| **Er** | 2.0 | 2.8 | 2.2 | 2.6 | 1.9 | 1.9 | 2.3 | 2.0 | 1.8 | 1.6 | 1.6 | 2.6 | 2.0 | 2.2 | 2.1 |
| **Tm** | 0.3 | 0.4 | 0.3 | 0.3 | 0.2 | 0.2 | 0.3 | 0.3 | 0.3 | 0.2 | 0.2 | 0.3 | 0.3 | 0.3 | 0.3 |
| **Yb** | 1.7 | 2.4 | 1.6 | 2.0 | 1.4 | 1.5 | 1.7 | 1.7 | 1.6 | 1.2 | 1.3 | 2.0 | 1.5 | 1.8 | 1.7 |
| **Lu** | 0.2 | 0.3 | 0.2 | 0.3 | 0.2 | 0.2 | 0.2 | 0.2 | 0.2 | 0.2 | 0.2 | 0.3 | 0.2 | 0.2 | 0.2 |
| **Hf** | 1.4 | 2.2 | 0.3 | 2.2 | 2.6 | 1.4 | 1.5 | 1.7 | 1.6 | 1.4 | 1.5 | 1.8 | 1.6 | 2.2 | 2.0 |
| **Ta** | 0.6 | 2.1 | 1.6 | 2.3 | 1.5 | 1.7 | 1.6 | 0.6 | 0.5 | 0.9 | 0.5 | 1.1 | 1.1 | 1.1 | 0.7 |
| **Pb** | 1.2 | 3.7 | 4.6 | 3.0 | 2.1 | 3.8 | 2.5 | 1.4 | 1.3 | 1.3 | 1.3 | 2.2 | 2.2 | 1.8 | 1.6 |
| **Th** | 1.3 | 5.1 | 5.6 | 4.8 | 3.3 | 4.7 | 3.1 | 1.1 | 1.1 | 1.6 | 1.3 | 2.9 | 2.7 | 2.3 | 1.7 |
| **U** | 0.4 | 1.6 | 1.7 | 1.6 | 0.9 | 1.4 | 0.9 | 0.2 | 0.1 | 0.3 | 0.3 | 0.7 | 0.4 | 0.6 | 0.4 |

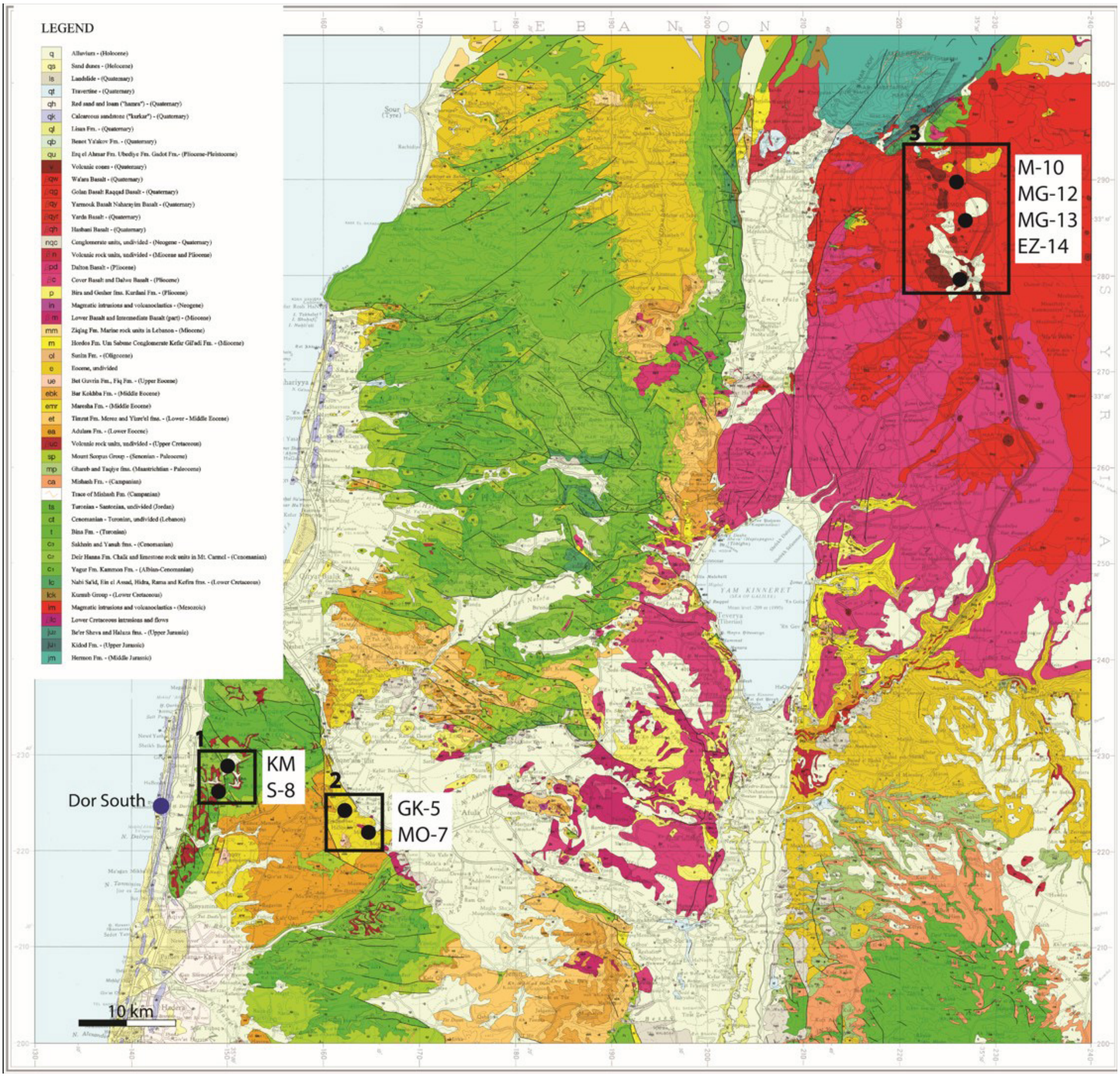


**Figure A.1.** Geological map of northern Israel (Sneh et al., 1997) showing locations of the site of Dor South (blue circle) and areas of basalt outcrops where geological references have been collected for this study: 1: Mount Carmel: Kerem Maharal (KM) and Shefeya (S-8); 2: Menashe Hills: Giv'at Kipod (GK-5) and Jezreel Valley: Midrach Oz (MO-7); 3: Golan Heights: Mas'ada (M-10), Merom Golan (MG-12, MG-13), and Ein Zivan (EZ-14).

---

## References

Brenner, I.B., Watson, A.E., Russell, G.M., Goncalves, M., 1980. A new approach to the determination of the major and minor constituents in silicate and phosphate rocks. *Chemical Geology* 28, 321–330. https://doi.org/10.1016/0009-2541(80)90052-2

Sneh, A., Bartov, Y., Rosensaft, M., 1997. *The Geological Map of Israel, 1:200,000, Sheet 1*. Israel Geological Survey, Jerusalem.

Yu, Z., Robinson, P., McGoldrick, P., 2001. An evaluation of methods for the chemical decomposition of geological materials for trace element determination using ICP-MS. *Geostandards and Geoanalytical Research* 25, 199–217. https://doi.org/10.1111/j.1751-908X.2001.tb00596.x

# Appendix B: Detailed pottery typology

Roey Nickelsberg and Assaf Yasur-Landau, Department of Maritime Civilizations, University of Haifa, Haifa, Israel (rnickelsberg@gmail.com)

Table B.1 shows 20 items that represent the studied pottery assemblage. Some of the items are illustrated in Figure 4 in the main article.

## Open vessels

A small open bowl (Fig. 4: 1) find parallels at ʻEn Esur and in Fazael 4 (Yannai, 2006: fig. 4.33.2; Bar et al., 2021: fig. 9.4), and a red-slipped platter/large shallow bowl (Fig. 4: 2) find parallels in Fazael 4 (Bar et al., 2021: fig. 13.5).

A pedestal bowl bearing a circular burn (soot) mark at its bottom (Fig. 4: 3) indicates its use as an incense burner. The base of this vessel shows the negative of one loop handle. Pedestal bowls found at ʻEn Esur have been associated with the Chalcolithic period (Yannai, 2006: fig. 4.25.3), yet they have no handles. Similar vessels with a handle have been discovered in the Yarmukian phases of Shaʻar Ha-Golan (Garfinkel, 1993: fig. 3.c4), and therefore it is possible that this item dates to the early Pottery Neolithic.

## Closed vessels

The Dor South assemblage consists mainly of storage jars (Fig. 4: 4–8) and holemouth jars (Fig. 4: 9–13) of varying forms.

### Storage Jars

The storage jars do not represent a tight EB IA assemblage. For example, a red-slipped and burnished straight-necked jar with a slightly outflaring rim (Fig. 4: 4) has parallels in an EB IA context in ʻEn Esur Area G (Yannai, 2006: fig. 4.68.2) but also in an EB IB context in ʻEn Esur Area B (Yannai, 2006: fig. 4.57.10), as well as in Fazael 4 (Bar et al., 2021: fig. 11.8). Another red-slipped and burnished jar (Fig. 4: 5), with a more pronounced outflaring rim has parallels in an EB IA context at ʻEn Esur (Yannai, 2006: fig. 4.38.16, 17). A red-slipped and burnished jar with a very short neck and a very slightly outflaring rim (Fig. 4: 6) can be compared with an EB IA example from ʻEn Esur (Yannai, 2006: fig. 4.37.7); however, similar jars are found also in Chalcolithic contexts (Yannai, 2006: fig. 4.22.4, 9). A straight-necked jar with an outflaring rim (Fig. 4: 7) seems to represent the later, EB IB, phase of the site, with parallels in an EB IB context at Tel Lod (van den Brink et al., 2015: fig. 24.4). A sherd probably belonging to a large storage jar or pithos bears a plastic rope decoration (Fig. 4: 18), which is common on large EB IA storage jars (Yannai, 2006: fig. 4.70.7; Bar et al., 2021: fig. 11.11).

### Holemouth Jars (Fig. 4: 9–13)

The holemouth jar fragments vary mostly in the shape of the rim and are all attributed to EB IA. These include two rims decorated with thumb indentations (Fig. 4: 9, 10) with parallels from ʻEn Esur, Ashqelon Afridar, and Fazael 4 (Yannai, 2006: fig. 4.43.11; Golani and Pasternak, 2020: fig. 8.9; Bar et al., 2021: fig. 10.16, respectively), two with a chamfered rim (Fig. 4: 11, 12; parallels: Yannai, 2006: fig. 4.43.3, 5; Golani, 2008: fig. 8.11), and one, red-slipped and burnished on the exterior and on the rim's interior, that has a squared rim (Fig. 4: 13; parallel: Yannai, 2006: fig. 4.43.13). Of these five examples, the first four are made of a light-brown paste with white inclusions, while the last is reddish. In general, most holemouth jar sherds from the site are light brown with white inclusions. Some holemouth jar fragments have traces of soot, possibly hinting at the use of these vessels in association with open fires.

### Handles

Two ledge handles (Fig. 4: 14, 15) have light thumb indents that are common in EB IA contexts (Golani, 2008: fig. 10.10; Golani and Pasternak, 2020: fig. 9.8, 10) and are usually located on storage and holemouth jars. In addition, a loop handle (Fig. 4: 16) and a small lug handle (Fig. 4: 17) in the assemblage may be associated with the Chalcolithic period (Yannai, 2006: fig. 4.17.20, 21); the latter came from the same basket as the pedestal bowl.

## Gray Burnished Ware (GBW)

The Gray Burnished Ware group is typical of EB I. Its main attribute is the distinctive gray color. Although only body sherds of this typological group were recovered at Dor South, some show distinctive markings indicating the vessel type, such as knobs, usually added to open vessels (Fig. 4: 19, 20; parallels: Yannai, 2006: figs. 4.17.20, 21; 4.49.3, 6).

**Table B.1.** The pottery assemblage (Fig. 4)

| No. | Basket | Type | Period | Description | Parallels |
|---|---|---|---|---|---|
| 1 | B19A5-2.6 | Bowl | EB IA | Orange material with light-brown/ gray core; red slipped and burnished exterior | Yannai, 2006: fig. 4.33.2; Bar et al., 2021: fig. 9.12 |
| 2 | B20A9-1.2 | Platter/ shallow bowl | EB IA | Light-brown/orange material with white inclusions; red paint visible on both exterior and interior | Bar et al., 2021: fig. 13.5 |
| 3 | B20A33-1.1 | Stand/ incense burner | Yarmukian/ Chalcolithic | Brown material with gray inclusions; round burnt mark in center of vessel's interior | Garfinkel, 1993: fig. 3.c4; Yannai, 2006: fig. 4.25.3 |
| 4 | B20A11-5.2 | Storage jar | EB IA/B | Light-brown material with dark-black core and gray inclusions; traces of red paint on exterior | Yannai, 2006: figs. 4.57.10, 4.68.2, 4.71.12; Bar et al., 2021: fig. 11.8 |
| 5 | B19A5-1.1 | Storage jar | EB IA | Light-orange color with dark-black core; red slip and burnish on exterior of jar and interior of rim | Yannai, 2006: fig. 4.38.16, 17 |
| 6 | B20A31-1.1 | Storage jar | Chalcolithic/ EB IA | Light-brown material with gray inclusions; red slip and burnish on exterior of jar and interior of rim | Yannai, 2006: figs. 4.37.7; 4.22.4, 9 |
| 7 | B20A11-5.3 | Storage jar | EB IB | Light-brown/orange material with gray inclusions | van den Brink et al., 2015: fig. 24.4 |
| 8 | B19A10-2.1 | Flat base | EB I | Light-brown/orange material with dark-black core; possible soot traces at bottom of base and red slip and burnish on base interior | |
| 9 | B19A18-2.3 | Holemouth jar | EB IA | Light-brown material with white/gray inclusions; possible soot traces outside; thumbed rope decoration around rim | Yannai, 2006: fig. 4.43.11; Golani and Pasternak, 2020: fig. 8.9; Bar et al., 2021: fig. 10.16 |
| 10 | B19A22-11 | Holemouth jar | EB IA | Light-brown material with white/gray inclusions; possible soot traces outside; thumbed rope decoration around rim | Yannai, 2006: fig. 4.43.11; Golani and Pasternak, 2020: fig. 8.9; Bar et al., 2021: fig. 10.16 |
| 11 | B20A35-1.1 | Holemouth jar | EB IA | Light-orange material with white and gray inclusions; red-painted rim | Golani, 2008: fig. 8.11 |

| No. | Basket | Type | Period | Description | Parallels |
|---|---|---|---|---|---|
| 12 | B20A11-5.1 | Holemouth jar | EB IA | Light-brown material with gray inclusions; possible red slip on rim | Yannai, 2006: fig. 4.43.3, 5 |
| 13 | B19A11-1.7 | Holemouth jar | EB IA | Light-brown material with white inclusions; red slip and burnish on exterior of vessel and interior of rim | Yannai, 2006: fig. 4.43.13 |
| 14 | B19A14-3.3 | Ledge handle | EB IA | Light-brown material with gray core and white inclusions | Golani and Pasternak, 2020: fig. 9.8, 10 |
| 15 | B19A14-3.5 | Ledge handle | EB I | Light-brown/orange material with dark core and white inclusions | Golani, 2008: fig. 10.10 |
| 16 | B20A9-1.3 | Handle | Chalcolithic | Dark-gray/reddish material with black inclusions | Yannai, 2006: fig. 4.10.4, 8 |
| 17 | B20A33-1.2 | Lug handle | Chalcolithic/ EB IA | Light-brown material with white inclusions; red slipped and burnished | Yannai, 2006: fig. 4.17.20, 21 |
| 18 | B20A9-1.1 | Rope decoration | EB IA | Light-brown material with white inclusions; plastic rope decoration. The sherd is painted red, with possible soot traces | Yannai, 2006: fig. 4.70.7; Bar et al., 2021: fig. 11.11 |
| 19 | B20A29-1.1 | GBW knob | EB IA | Dark-gray material; knob-shaped plastic decoration typical of GBW vessels | Yannai, 2006: fig. 4.49.3 |
| 20 | B19A10-1.1 | GBW knob | EB IA | Light-gray material with dark-gray inclusions; knob-shaped plastic decoration typical of GBW vessels | Yannai, 2006: fig. 4.49.6 |

## References

Bar, S., Zutovski, K., Hruby, K., Ujma, C., 2021. Excavations at the Early Bronze Age I site Fazael 4: the 2017–2020 seasons. *Journal of the Israel Prehistoric Society* 51, 261–303.

Garfinkel, Y., 1993. The Yarmukian culture in Israel. *Paléorient* 19 (1), 115–134.

Golani, A., 2008. The Early Bronze Age site of Ashkelon, Afridar—Area M. *'Atiqot* 60, 19–51.

Golani, A., Pasternak, M.D., 2020. Ashqelon Afridar, Area O-2: Early Bronze Age IA remains. *Hadashot Arkheologiyot–Excavations and Surveys in Israel* 132, 1–23. https://www.hadashot-esi.org.il/report_detail_eng.aspx?id=25875&mag_id=128

Brink, E.C.M. van den, Horwitz, L.K., Kool, R., Liphschitz, N., Mienis, H.K., Zbenovich, V., 2015. Excavations at Tel Lod: remains from the Pottery Neolithic A, Chalcolithic, Early Bronze Age I, Middle Bronze Age I and Byzantine periods. *'Atiqot* 82, 141–218.

Yannai, E., 2006. *'En Esur ('Ein Asawir)*, I: *Excavations at a Protohistoric Site in the Coastal Plain of Israel* (IAA Reports 31). Israel Antiquities Authority, Jerusalem.

# Appendix C: Detailed results of phytolith morphotype analysis

Shira Gur-Arieh, Leon Recanati Institute for Maritime Studies, University of Haifa, Israel, Department of Maritime Civilizations, School of Archaeology and Maritime Cultures, University of Haifa, Israel (shiragura@gmail.com)

The results presented below are based on a minimum of 200 individual phytoliths described morphologically for each sample, using Madella et al. (2005) and International Committee for Phytolith Taxonomy (ICPT) (2019). In addition to the individual phytoliths, multicells (MCs) were noted separately and later added to the total number of phytoliths. This enabled to keep track of the number of MCs in each sample and their size range, while avoiding a morphological bias arising from the inclusion of only a small variety of morphotypes in samples rich in large MCs. Table C.1 presents basic data, while Table C.2 presents the raw results.

Figure C.1 shows the dominance of monocotyledonous phytoliths in the studied six samples, while Figure C.2 presents the high proportion of inflorescence relative to leaf/stem monocotyledonous phytoliths. The latter indicates that monocots were utilized during spring and summer, when grasses flower, and more probably year-round.

Figure C.3 presents the percentages of the different short cells from the total short cell counts, showing that most of the grass short cells originate in $C_3$ pooid (festucoid) grasses (65.52–90.00% rondel and trapeziform phytolith morphotypes), while $C_4$ chloridoid (saddle morphotypes) and $C_4$ panicoid (lobate and cross morphotypes) are present in lower proportions.

One sample from Layer 2 includes an irregular verrucate multicell, possibly originating in *Celtis* sp. seed coats (Rodríguez-Cintas and Cabanes, 2017).

**Table C.1.** Details on sediment samples analyzed: stratigraphic context, sample number, phytolith concentration, sum of phytoliths used for morphometric analysis, and total count of multicell phytoliths per sample

| Layer no. (general description) | Sample no. | Phytolith concentration (millions/1g sediment) | No. of phytoliths analyzed | Total no. of MCs |
|---|---|---|---|---|
| 2 (lower gray deposit) | S20A-5-2 | 36 | 311 | 86 |
| | B20A-35-3 | 43 | 310 | 77 |
| 3 (middle brown deposit) | S20A-3-6 | 10 | 289 | 58 |
| | S20A-5-3 | 7 | 320 | 83 |
| 4 (upper gray deposit) | S20A-1-1 | 29 | 351 | 95 |
| | S20A-4-5 | 28 | 290 | 44 |

**Table C.2.** Results of the phytolith morphotype analysis

| Botanical categories | Phytolith morphotypes | Sediment samples | | | | | |
|---|---|---|---|---|---|---|---|
| | | S20A1-1 | S20A4-5 | S20A3-6 | S20A5-3 | S20A5-2 | SB20A35-3 |
| Dicot leaf | Dicot hair | | | | | 1 | 1 |
| | Unciform hair | | | | | 6 | |
| | Jigsaw puzzle | 3 | | 4 | 2 | | |
| Dicot wood/bark | Discoid rugulate | | | 1 | | | |
| | Discoid psilate | | | | 1 | | |
| | Ellipsoid echinate | | | 1 | | | 1 |
| | Ellipsoid psilate | | 1 | | | 2 | |
| | Ellipsoid rugulate | 1 | | | 1 | | |
| | Irregular psilate | 5 | 6 | 9 | 6 | 2 | 1 |
| | Irregular rugulate | 6 | 2 | 6 | 3 | | 2 |
| | Parallelepiped blocky psilate | | 8 | 6 | 5 | 3 | 3 |
| | Parallelepiped blocky rugulate | 3 | 2 | 5 | 3 | 1 | |
| | Parallelepiped thin psilate | 3 | 3 | 1 | | 1 | |
| | Parallelepiped thin rugulate | | 1 | 1 | | 1 | 1 |
| | Platelet | | 1 | 1 | 1 | 1 | |
| | Spheroid psilate | 1 | | 1 | 1 | | |
| | Spheroid rugulate | 2 | 1 | 2 | | 1 | |
| General monocot | Cylindroid echinate | 9 | 3 | 6 | 3 | 3 | 1 |
| | Cylindroid psilate | 21 | 11 | 8 | 23 | 16 | 10 |
| | Cylindroid rugulate | 15 | 10 | 10 | 17 | 21 | 8 |
| | Cylindroid sinuous | 4 | 3 | | 1 | 2 | |
| | Long cell polylobate | | 4 | 1 | | | |
| | Long cell sinuous | 12 | 15 | 12 | 3 | 19 | 12 |
| | Long cell wavy | 6 | 9 | 13 | 5 | 2 | 8 |
| Monocot leaves/ stems | Bulliform cell cuneiform | 9 | 6 | 3 | 3 | 1 | 3 |
| | Bulliform cell parallelepipedal | 6 | | 2 | 1 | 1 | |
| | Parallelepiped elongate psilate | 19 | 7 | 22 | 49 | 27 | 27 |
| | Parallelepiped elongate rugulate | 11 | 7 | 13 | 24 | 5 | 33 |
| | Mesophyll | | 1 | | | | |
| | Prickle | 8 | 15 | 7 | 12 | 6 | 2 |
| | Stomata | | | | | 1 | |
| Monocot inflorescences | Hair | 2 | | | 1 | | |
| | Long cell dentritic | 55 | 48 | 25 | 47 | 48 | 62 |
| | Long cell echinate | 37 | 33 | 39 | 35 | 37 | 52 |
| | Long cell verrucate | 43 | 31 | 31 | 19 | 29 | 22 |
| | Papillae | 13 | 7 | 3 | 12 | 11 | 4 |
| Grass short cells | Short cell bilobate | 3 | 4 | 2 | 1 | | 5 |
| | Short cell polylobate | 1 | 1 | 1 | | | |
| | Short cell saddle | 5 | 7 | 1 | 2 | 11 | 8 |
| | Short cell cross shaped | 1 | | | | | 1 |
| | Short cells rondel | 14 | 21 | 30 | 16 | 31 | 25 |
| | Short cell rondel tower | | | | | | 2 |
| | Short cell trapeziform | 5 | 4 | 6 | 2 | 3 | 4 |

| Botanical categories | Phytolith morphotypes | Sediment samples | | | | | |
|---|---|---|---|---|---|---|---|
| | | S20A1-1 | S20A4-5 | S20A3-6 | S20A5-3 | S20A5-2 | SB20A35-3 |
| Family specific | Cyperaceae (sedges) | 1 | | | 1 | 11 | 5 |
| | Spheroid echinate (palm) | | | 1 | | | |
| | MC irregular verucate (*Celtis*) | | | | | | 7 |
| Other | Weathered | 26 | 18 | 15 | 20 | 7 | |
| | Melted | 1 | | | | | |
| | Fragment | 25 | 5 | 18 | 14 | 9 | 45 |
| | Fusiform diatom | | | | | | 2 |
| | Sponge spicule | | 1 | 1 | 1 | | |
| Total | Total | 351 | 290 | 289 | 320 | 311 | 310 |
| | non identified | 5 | 6 | 5 | 2 | 3 | |
| | MC cylindroid psilate | | | | | | |
| | MC cylindroid echinate | 2 | | | | | |
| | MC long cell dentritic | 29 | 22 | 13 | 20 | 34 | 22 |
| | MC long cell echinate | 3 | 5 | 6 | 7 | 12 | 9 |
| | MC long cell psilate | 10 | | 12 | 30 | 16 | 7 |
| | MC long cell rugulate | 11 | 5 | 8 | 14 | 2 | 23 |
| | MC long cell wavy | 3 | 8 | 11 | 4 | | 4 |
| | MC long cell sinous | | | 2 | | 4 | |
| | MC no identified | 5 | 2 | | 1 | | |
| | Jigzaw puzzle | 3 | | 4 | 2 | | |
| | MC papillae | 2 | | | 3 | 6 | |
| | MC dendritic + papillae | 10 + 7 | 7 + 3 | 2 + 1 | 11 + 3 | | |
| | MC verucate | 12 | | | 2 | 9 | 5 |
| | MC Cyperaceae | | | | | 3 | |
| | MC bulliform parallelepipedal | 5 | | 2 | | | |
| | MC spheroid rogulate | 2 | | | | | |
| | MC long cell parallelepiped psilate thin | 2 | 2 | | | | |
| | MC bulliform cuneiform | 6 | | | | | |
| | MC elongated psilate + prickle | | | | 3 + 1 | | |
| | MC dendritic + short cell not identified | | | | | | 18 + ? |
| | MC echinate + papillae | | | | | | 2 + 1 |
| | MC celtis | | | | | | 7 |
| | MC wavy + rondel | | | | | | 2 + 1 |
| | Total phytoliths in MC | 95 | 44 | 58 | 83 | 86 | 77 |
| | %MC | 27.07 | 15.17 | 20.07 | 25.94 | 27.65 | 24.84 |
| MC | Small (2–4) | 28 | 17 | 20 | 20 | 19 | 19 |
| | Medium (5–10) | 6 | 2 | 1 | 6 | 5 | 5 |
| | Large (11–20) | | | | 1 | 1 | 2 |
| | Huge (> 20) | | | | | | |
| | Total MC | 34 | 19 | 21 | 27 | 25 | 26 |

| | Summary data | S20A1-1 | S20A4-5 | S20A3-6 | S20A5-3 | S20A5-2 | SB20A35-3 |
|---|---|---|---|---|---|---|---|
| | **% Monocot (from total)** | 85.19 | 85.17 | 81.31 | 86.25 | 88.10 | 93.23 |
| | **% Dicot (from total)** | 6.84 | 8.62 | 13.15 | 7.19 | 6.11 | 2.90 |
| | **% Other (from total)** | 0.28 | 0.00 | 0.35 | 0.31 | 3.54 | 3.87 |
| | **% Weathered (from total)** | 7.41 | 6.21 | 5.19 | 6.25 | 2.25 | 0.00 |
| | **% Melted (from total)** | 0.28 | 0.00 | 0.00 | 0.00 | 0.00 | 0.00 |
| | **% Monocot inflorescence (from total)** | 42.74 | 41.03 | 33.91 | 35.63 | 40.19 | 45.16 |
| | **% Monocot leaves/stems (from total)** | 15.10 | 12.41 | 16.26 | 27.81 | 13.18 | 20.97 |
| | **% Inflorescence (from sum inflo. + leaves/stems)** | 73.89 | 76.77 | 67.59 | 56.16 | 75.30 | 68.29 |
| | **% Leaves/stems (from sum inflo. + leaves/stems)** | 26.11 | 23.23 | 32.41 | 43.84 | 24.70 | 31.71 |
| | **% leaves/inflorescences** | 0.35 | 0.30 | 0.48 | 0.78 | 0.33 | 0.46 |
| | **% Festucoid (from total)** | 5.41 | 8.62 | 12.46 | 5.63 | 10.93 | 10.00 |
| | **% Panicoid (from total)** | 1.42 | 1.72 | 1.04 | 0.31 | 0.00 | 1.94 |
| | **% Chloridoid (from total)** | 1.42 | 2.41 | 0.35 | 0.63 | 3.54 | 2.58 |
| | **% All short cells (from total)** | 8.26 | 12.76 | 13.84 | 6.56 | 14.47 | 14.52 |
| | **% Festucoid (from short cells)** | 65.52 | 67.57 | 90.00 | 87.71 | 75.56 | 68.89 |
| | **% Panicoid (from short cells)** | 17.24 | 13.51 | 7.50 | 4.76 | 0.00 | 13.33 |
| | **% Chloridoid (from short cells)** | 17.24 | 18.92 | 2.50 | 9.52 | 24.44 | 17.78 |
| | **% Long cell dendritics** | 15.67 | 16.55 | 8.65 | 14.69 | 15.43 | 20.00 |
| | % Long cells echinates | 10.54 | 11.38 | 13.49 | 10.94 | 11.90 | 16.77 |

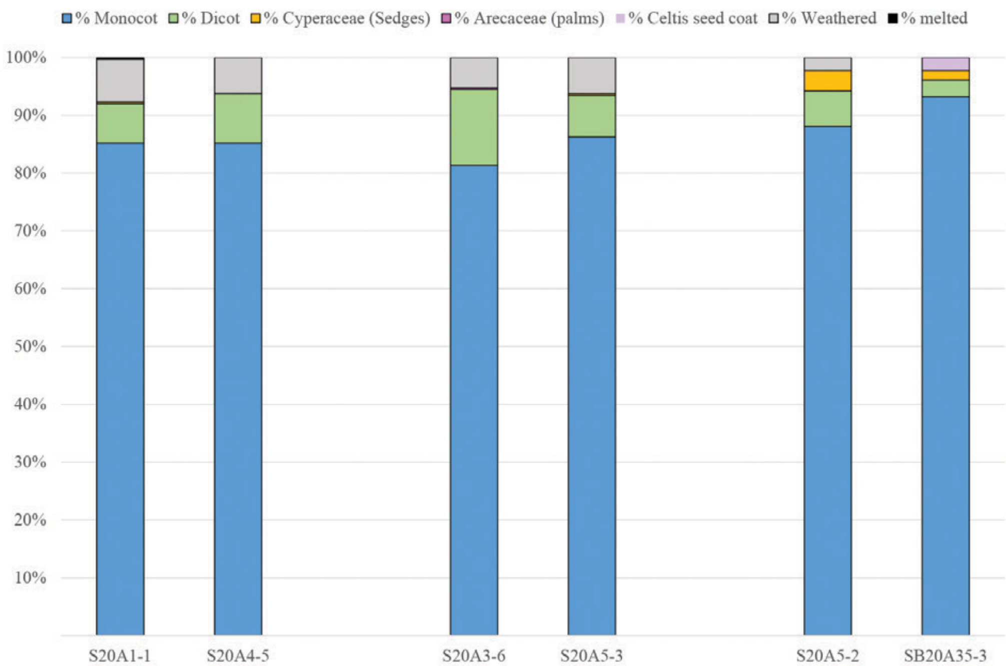


**Figure C.1.** Relative proportions of monocot, dicot, sedges, palms, *Celtis* seed coat, weathered, and melted phytoliths. The low percentage of weathered and melted phytoliths indicates well-preserved phytolith assemblages.

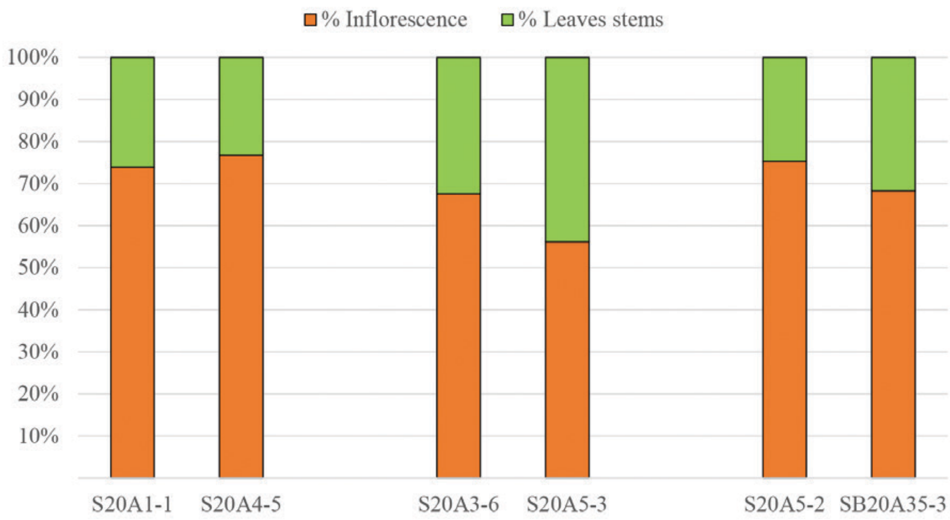


**Figure C.2.** The relative proportions of long cell phytoliths from inflorescence and those from leaves and stems, out of the total monocot long cell phytoliths identified. Note the high relative proportion of monocot inflorescence phytoliths.

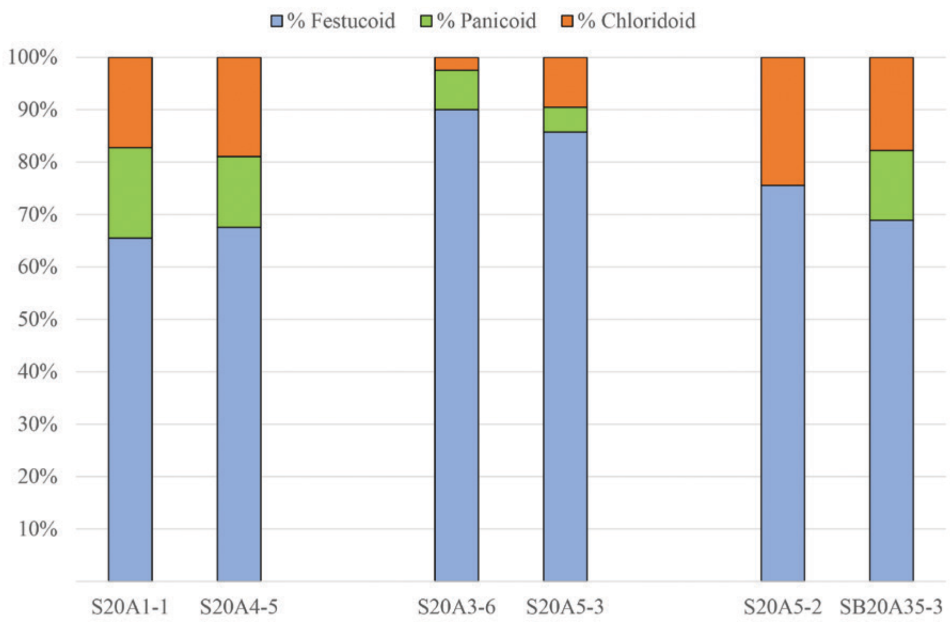


**Figure C.3.** Proportions of short cells from the three grass subfamilies out of the total number of short cells in the studied phytolith assemblages. Note the higher proportion of $C_4$ grasses in the sediments from Layers 2 and 4, while the sediments from Layer 3 are dominated by $C_3$ grass phytoliths.

## References

Madella, M., Alexandre, A., Ball, T., 2005. International Code for Phytoliths Nomenclature 1.0. *Annals of Botany* 96 (2), 253–260. https://doi.org/10.1093/aob/mci172.

International Committee for Phytolith Taxonomy (ICPT), 2019. International Code for Phytolith Nomenclature (ICPN) 2.0. *Annals of Botany* 124 (2), 189–199. https://doi.org/10.1093/aob/mcz064.

Rodríguez-Cintas, A., Cabanes, D., 2017. Phytolith and FTIR studies applied to combustion structures: the case of the Middle Paleolithic site of El Salt (Alcoy, Alicante). *Quaternary International* 431 (A), 16–26. https://doi.org/10.1016/j.quaint.2015.09.043.

# Appendix D: Quantitative summary of the flint assemblage

Gal Bermatov-Paz, Department of Maritime Civilizations, University of Haifa
(gbermatov@staff.haifa.ac.il)

A total of 1415 flint items were analyzed; this assemblage comprises 228 flint chunks and 1187 worked items (Table D.1).

**Table D.1.** General breakdown of the flint assemblage from Dor South

| Type | No. | % |
|---|---|---|
| Flakes | 551 | 46.4% |
| Blades | 47 | 4.0% |
| Bladelets | 56 | 4.7% |
| Core trimming elements | 63 | 5.3% |
| Primary elements | 199 | 16.8% |
| Cores | 121 | 10.2% |
| Tools | 139 | 11.7% |
| Burin spalls | 11 | 0.9% |
| **Subtotal** | **1,187** | **100.0%** |
| Chunks | 228 | |
| **Total** | **1,415** | |

Tools (n = 139) account for 11.7% of the worked items (Table D.2).

**Table D.2.** General breakdown of the tool assemblage found at Dor South

| Type | No. | % |
|---|---|---|
| Perforators | 15 | 10.8% |
| Bifaces | 5 | 3.6% |
| Backed pieces | 12 | 8.6% |
| Burins | 6 | 4.3% |
| Carinated | 1 | 0.7% |
| Composite | 3 | 2.2% |
| Notched & denticulated | 21 | 15.1% |
| Geometrical microliths | 2 | 1.4% |
| Microliths | 4 | 2.9% |
| Retouched pieces | 54 | 38.8% |
| Scrapers | 10 | 7.2% |
| Truncated | 6 | 4.3% |
| **Total** | **139** | **99.9%**[1] |

[1] Percentages do not add up to 100 due to rounding.

# Appendix E: Special finds

Gal Bermatov-Paz, Department of Maritime Civilizations, University of Haifa
(gbermatov@staff.haifa.ac.il)

Three items made of rock were found in secure contexts: B20A-24-3: A black fragment of a polished and perforated round item from Layer 3, made of hematite (Fig. E.1: 1).
B20A-41-3: A polished dark red-purple weight from Layer 3, made of an unknown silicate rock (Fig. E.1: 2).
B20A-10-4: A round black weight (probably a loom weight) from Layer 4, made of vesicular basalt (Fig. E.1:

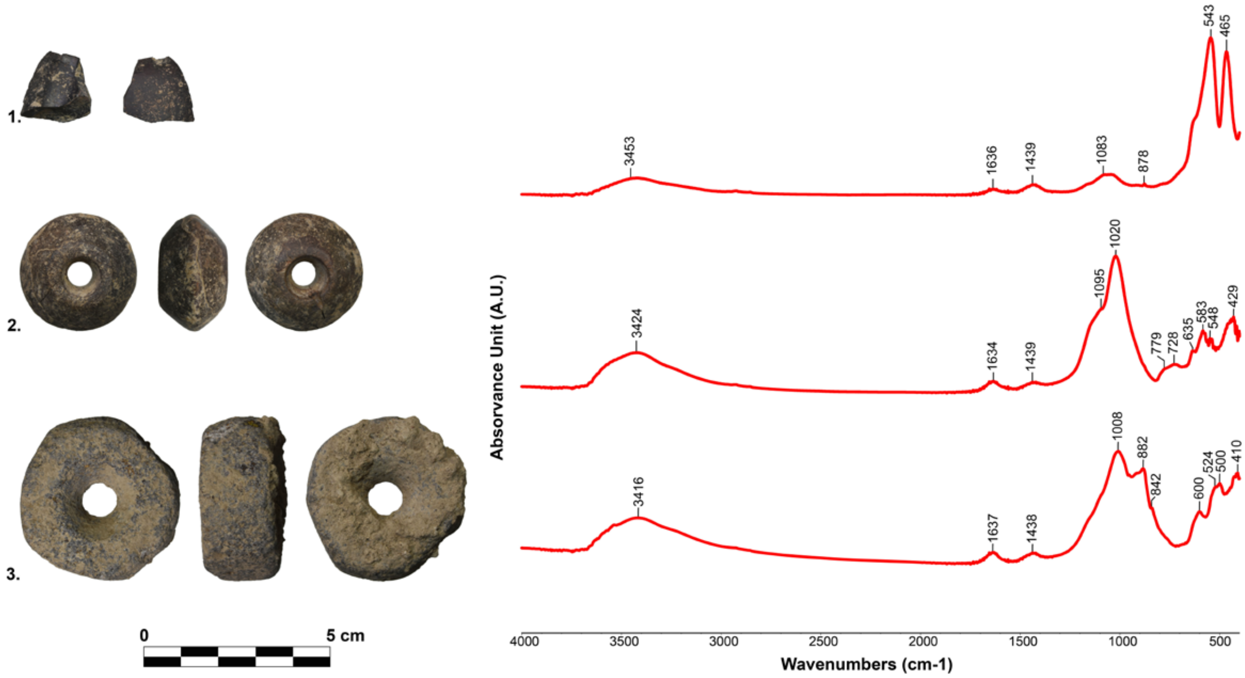


**Figure E.1.** Special finds from Dor South. The FTIR spectra on the right accord with the items' images on the left.

# Appendix F: Context information for micromorphology block analysis

Ruth Shahack-Gross, Department of Maritime Civilizations, University of Haifa
(rgross@univ.haifa.ac.il)

Figure F.1 provides the context information for the blocks used to illustrate the micromorphological characteristics of the site's deposits that appear in the main text.

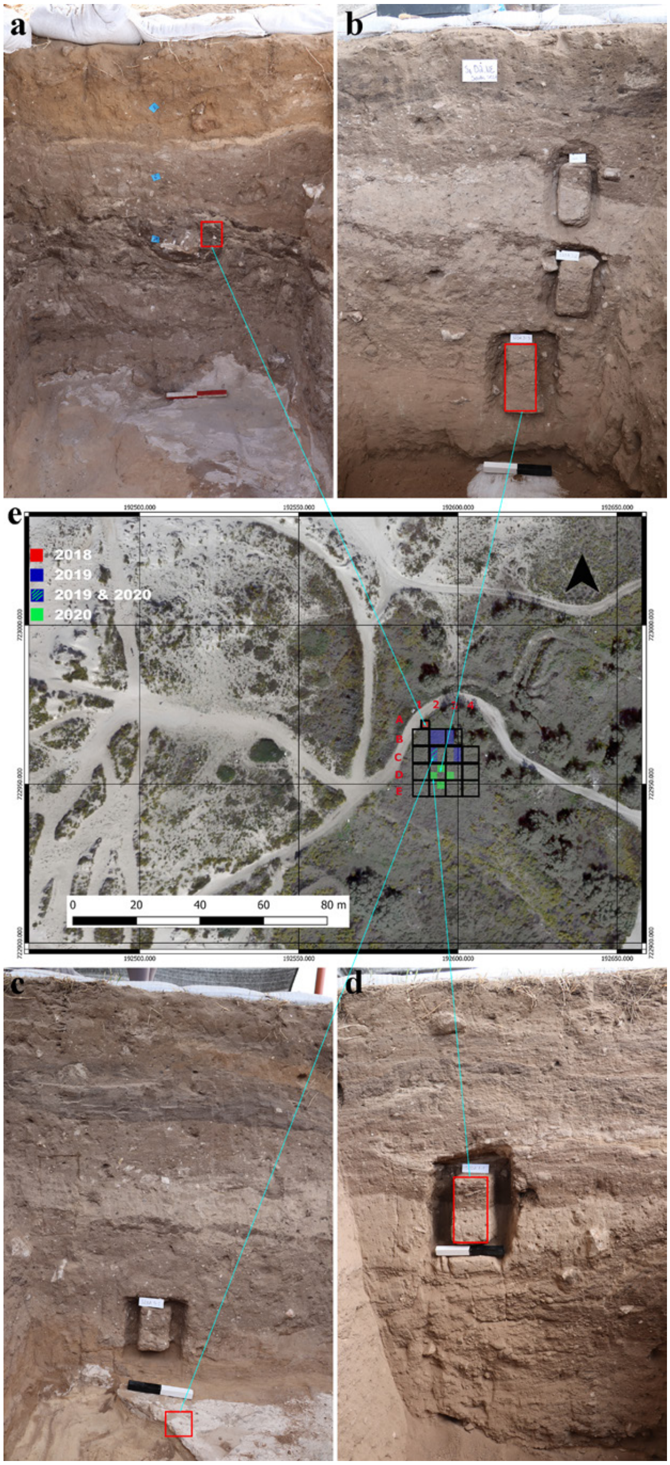


**Figure F.1**. Position of the blocks (marked by red rectangles) (a–d) and their location on the site's grid (marked by blue arrows) (e); red-white scale bar in section photos is 20 cm long; black-white scale bar is 10 cm long. Block DS18A-2-4 from the 2018 season, Square A1, southern section, dark-brown sandy mud-brick material (Layer 3) (a); Block DS20A-3-3 from the 2020 season, Square D2 NE, southern section, grayish-brown sediment (Layer 3) and slightly lighter grayish-brown sediment below it (Layer 2) (b); Block DS20A-5-3 from the 2020 season, Square C2 W, southern part, white cemented sterile deposit (Layer 1) (c); Block DS20A-4-1 from the 2020 season, Square D2 SW, southern section, gray fine sediment (Layer 4) and dark-brown sediment above it (Layer 5) (d).